3-D Deployment of VLC Enabled UAV Networks with Energy and User Mobility Awareness

Dil Nashin Anwar, *Member, IEEE*, Mansi Peer, Kanak Lata, Anand Srivastava, *Member, IEEE*, and Vivek Ashok Bohara, *Member, IEEE*

***Abstract*—The recent proliferation of light-emitting diodes (LEDs) in unmanned aerial vehicles (UAVs) for inspection, first response, environmental protection monitoring, surveillance and urban safety especially at night time, have paved the way for visible light communication (VLC) enabled UAVs. Since UAVs are power limited and size constrained devices, the utilization of visible light for communication and illumination in UAVs help in reducing energy and air-frame cost. Further, when the ground users are mobile, UAV placements require regular updates at optimized update intervals. Consequently, we propose energy and user mobility aware three-dimensional (3-D) deployment of VLC enabled UAV-base station (UB_v) so that maximum coverage of users while ensuring fairness is achieved. The farthest user and shifting UAV based solutions have been proposed for the joint optimization of UB_v placement and the update interval. The complexity of the proposed approaches is lower than the exhaustive-search based solution, thus, making the UB_v network energy-efficient. The UB_v coverage area to serve ground users has been enhanced with holographic light-shaping diffusers (LSD). The optimum angle of the LSD has been obtained based on LED optical transmitted power and desired UB_v maximum coverage. A novel red, green and blue (RGB) LED solution based on light sensitivity to the human eye is proposed to increase the coverage area for the night scenario. Moreover, we derive the analytical expressions to determine the maximum coverage radius and UB_v optimum altitude for the defined quality-of-service (QoS) metrics. Finally, the proposed UB_v network is evaluated in terms of update instant, service time and effective users covered.**

***Index Terms*—Visible Light Communication (VLC), Unmanned Aerial Vehicle (UAV), holographic light shaping diffuser (LSD), RGB LED, User Mobility, Coverage Probability**

I. INTRODUCTION

THE demand for unmanned aerial vehicles (UAVs) have been snowballing over the last few years. The real-time aerial video transmission is one of the myriad applications of wireless communication through UAVs, which is conventionally utilized for remote sensing, surveillance, aerial inspection, and monitoring [1]. UAVs can also be deployed as aerial base stations (BSs) or relays in communication networks [1], [2]. These aerial base stations are referred to as UAV-BS. UAV-BSs can augment the performance of desired communication network owing to their high mobility, maneuverability in the three-dimensional (3D) space, fast deployment and ease of accessibility in remote areas.

Wireless communication based on radio frequency (RF) faces a spectrum crunch due to increased demand on its limited bandwidth. Therefore, visible light communication (VLC) can play a significant role as it provides ample unlicensed bandwidth and offers various advantages such as free from electromagnetic interference, utilization of existing illumination infrastructure to support green communication, along with high level of security over RF communication [3], [4]. VLC relies on light-emitting diode (LEDs) for signal transmission which makes them particularly suitable for scenarios like search and rescue in which both illumination and communications are required. LEDs outperform the other light sources with their high electrical-to-optical conversion efficiency, long life span, small size, light weight, low cost and modulation performance [5]. Therefore, the energy-efficient LEDs further reinforce the emerging VLC technology. Further, the authors in [6] have proposed the concept of integrating LEDs in UAVs, for illumination in applications such as disaster recovery and urban safety. For night time UAV operations, Draganfly Innovations [7] are designing and manufacturing UAVs equipped with LEDs. Therefore, the recent use of LED mounted on a UAV inspires the researchers to combine VLC and UAVs to provide simultaneous communication and illumination for inspection, environmental protection monitoring, first response, urban safety especially at night and emergency communication for disaster recovery [6], [8], [9]. The active interest in VLC enabled vehicular networks has further pushed the research in VLC enabled UAVs, which can satisfy the dual requirement of illumination as well as communication of ground users through visible light. Further, above mentioned utilization of LEDs in UAVs for communication and illumination eliminate the extra cost and energy required in UAVs for RF-based communication [10], [11]. Owing to the numerous advantages of VLC, VLC-enabled UAV-BS (UB_v) communications can become a promising technology. However, three-dimensional (3-D) placement of UB_v is one of the crucial challenges in UAV-assisted communication networks [1], [2].

A. Literature Review and Motivation

Deployment of UB_v networks is challenging, as it depends on many factors such as deployment environment e.g., geographical area, locations of ground users, air-to-ground channel characteristics, etc. The literature is replete with RF-based UAV-BS (UB_r) networks and its deployment. The optimized deployment of static and mobile UB_r has been discussed in [12]. In case of static UB_r deployment, the position of UB_r remains same for the entire duration of operational time whereas for mobile UB_r, the deployment position changes many times during allotted operational time [13]. However, for vertical deployment in UB_v, one cannot consider the same height as UB_r since in UB_v the aim is to simultaneously

This paragraph of the first footnote will contain the date on which you submitted your paper for review.

The authors are from Department of Electronics and Communication Engineering, IIIT-Delhi, India (correspondence e-mail:dilnashina@iiitd.ac.in)

provide communication and illumination. In case of UB_r, the altitude is mostly fixed based on certain communication parameters such as achievable data rate, error rate or signal-to-noise ratio (SNR). Therefore, a plethora of works in RF-equipped UAVs are for two-dimension (2-D) deployment. However, in UB_v, the vertical deployment depends on two factors communication and illumination especially for night scenario or say low light scenarios. Further, VLC channel gain is different from the RF channel gain. Therefore, UB_v can not be deployed at the same altitude as of UB_r. Secondly, for the user mobility aware 2-D deployment one may expect that similar deployment technology can be used for both UB_r and UB_v. However, the maximum coverage radius changes for UB_v from UB_r because the altitude and quality-of-service (QoS) metrics are different in both cases.

Next, we would like to emphasize on the novel optimization problem being solved in this work: a joint optimization of the UB_v 3-D positioning and the update interval has been proposed to maximize the number of covered users with VLC specific QoS constraints (i.e., illumination and reliable communication) at an update instant by ensuring user fairness and flight time constraint. In [14], the joint optimization of the UB_r 2-D positioning and the update interval has been done with the standard exhaustive search based strategy (ES) algorithm integrated with the greedy approximate approach [15] which is extended to UB_v deployment in our work. Further, the optimization of UB_r deployment becomes even more challenging when mobility of ground users is taken into consideration as it requires multiple updates based on the user mobility [16]. A reinforcement-learning (RL) based technique has been utilized for dynamic heterogeneous network to update the UB_r deployment [17]. In [18], a multi-agent Q-learning based algorithm is used to obtain the UB_r trajectory which is based on the prediction of users' position. In [19], RL technique has been adopted in fair maximum coverage deployment of UAVs, where the convergence of the proposed algorithm takes training episodes of the order of 10^4. The time complexity of RL depends on its training convergence. Further, highly complex algorithms are less preferred for UB_v networks owing to the power limitations and size constraints of UAVs. Therefore, motivated by the aforementioned issues, this paper presents two energy-aware algorithms (i.e., farthest user based strategy (FU) and shifting UAV based strategy (SU)) to achieve performance close to the exhaustive one whilst reducing the complexity. The focus of this work is to minimize flight time of UB_v and maximize coverage probability of users with energy-aware and low complex methods. Concept of fixed update interval has been introduced in [16] and [18] to quantify the repeated updates for mobile UB_r. However, there is a lack of literature on UB_vs which takes into account the flexibility of update interval, flight time, service time and coverage probability together with user mobility awareness. In [20], the multi-UAV-based heterogeneous flying ad hoc networks (FANET) has been surveyed with more focus on the concept of gateways in the network to connect small and mini UAVs via a communication network, whereas in this work the focus is on the reliable communication between UB_v and mobile ground users. Additionally, two of the challenges and open issues presented in [20] have been investigated in this work for UB_v, which is mobility modelling of UB_v with user mobility awareness and energy-efficient scheme.

The existing work in UB_v system primarily focuses on its power efficient deployment. In a multi-UB_v, multi-user scenario, to jointly satisfy the users' data rate and illumination, location of UB_vs and the cell associations (different sub-regions corresponding to the deployed UB_vs) are optimized under illumination and communication constraints in [8]. However, effect of interaction among different UB_vs has not been considered. In [9], interaction amongst different UB_vs is taken into account. An optimization problem is formulated to improve the performance by minimizing the transmit power consumption of interacting UAVs to meet different data rate and illumination requirements of ground users. The work in [21] describes the deep learning (DL) based approach for power efficient deployment of UB_vs. Specifically, they use a machine learning framework of gated recurrent units (GRUs) with convolutional neural networks (CNNs) to model the long-term historical illumination distribution and predict the future illumination distribution of the ground users. In these works the power efficient deployment of UAVs has been done in 2-D with fixed altitude of UB_v. However, in our proposed work the 3-D UB_v deployment has been done to cover maximum number of mobile users with low complexity. The work in [22] discusses integration of non-orthogonal multiple access (NOMA) with UB_vs to realize massive connectivity requirement for 5G and beyond. This technique also helps to serve more users compared to the VLC system without NOMA. A joint problem of power allocation and UB_v's placement is solved to maximize the sum rate of all users, subject to constraints on power allocation, QoS of users as well as UB_v's position. Nevertheless, the benefit of multiple access provision in UB_vs comes at the cost of higher complexity. UB_vs meant for communication should avoid lag and latency, therefore most of the decision should be taken by UB_vs only. Since, UAVs in general are resource constrained devices, therefore the aim of this paper is to reduce the complexity of computing the optimal UB_v placement to cover maximum possible users with energy awareness. The research aim in most of the prior work is to reduced power requirement at UB_v. However, the 3-D deployment of UB_v so as to maximize the number of covered users and minimize the UB_v flight time with energy and user mobility awareness has not been studied before. Further, no existing work in UB_v has considered the variation of day and night scenario in coverage. This paper for the very first time investigates UB_v coverage radius with respect to its altitude to provide reliable communication for day scenario, and both reliable communication and illuminance for night scenario. Further, energy-aware techniques have been proposed to enhance the maximum coverage radius of UB_v. A novel RGB LED solution based on light sensitivity to human eye have been proposed specific to night scenario which increases the coverage radius by increasing the illuminance, thereby supporting green communication. For both day and night scenarios, the coverage radius has been increased with the inclusion of holographic light shaping diffuser (LSD) [23]–[25] as LED front end. The optimum angle of the LSD has been obtained based on the LED optical transmit power to achieve maximum coverage radius and its optimum altitude

This article has been accepted for publication in a future issue of this journal, but has not been fully edited. Content may change prior to final publication. Citation information: DOI 10.1109/TGCN.2022.3171920, IEEE Transactions on Green Communications and Networking

for the desired QoS metrics. Further, the 3-D deployment of UB_v in an outdoor scenario provides flexibility to vary altitude (L) of UB_v for enhancing the coverage radius (r). Therefore, the proposed work thoroughly investigates the relationship between L and r which has not been extensively studied in literature for a UB_v network. This work is first of its kind to derive and provide the theoretical expressions of enhanced coverage radius as a function of L for the two QoS metrics to ultimately obtain optimal altitude and its respective maximum coverage radius analytically.

B. Contributions

The key contributions of the proposed work can be summarized as follows:

1) In this work, the altitude deployment of UB_v have been optimized for maximum coverage of ground mobile users while fulfilling illumination and reliable communication requirements.
2) The maximum coverage radius has been enhanced with energy-aware techniques: novel RGB LED based solution and holographic LSD. The analytical solution for optimum coverage radius with the proposed techniques has been derived.
3) A joint optimization of the UB_v 2-D positioning and the update interval has been proposed to maximize the number of covered users with VLC specific QoS constraints at an update instant by ensuring the user fairness as well as UB_v flight time constraint.
4) This paper proposes two energy-aware solutions based on farthest user and shifting strategy for the above mentioned joint optimization problem. The proposed methods have been compared with the standard exhaustive search based strategy.

The rest of the paper is organized as follows. Section II presents the UB_v network model and QoS metrics. Section III formulates the problem and discusses the solution. Section IV discusses the results obtained. Finally, Section V concludes the paper with future work directions. Table I summarizes the notations, acronyms and abbreviations used throughout the paper.

II. VLC ENABLED UAV NETWORK MODEL

In literature, mainly two types of UAVs have been considered, i.e., multirotor (or rotary UAVs) and fixed-wing UAVs. Rotary UAVs have greater manoeuvrability, compact design, and are easy to control and fly in any direction, whereas fixed-wing UAVs are less manoeuvrable, cannot hover, but can provide increased range and payload capacity [26], [27]. Therefore, rotary UAVs become more suitable for communication and illumination purposes because of their greater manoeuvrability and ability to hover in a stationary position. Further, the reduced range of rotary UAVs is not an issue as UB_v are capable of providing service only within a small area (in hundreds of meters). However, it is crucial to reduce the energy consumption in rotary UAVs due to their limited energy. Therefore, energy-efficient schemes are required for the 3-D deployment of rotary UAVs.

We consider a UB_v network model which serves N mobile ground users as shown in Fig. 1. The total operating time

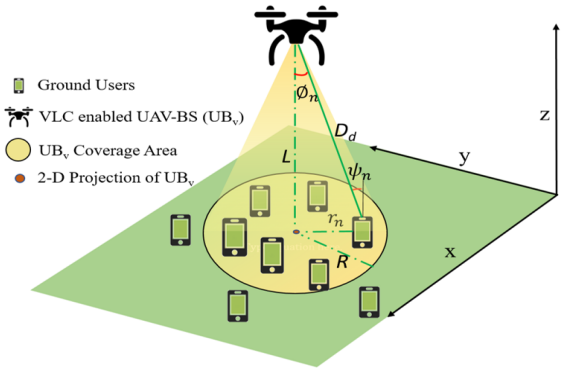

Fig. 1. VLC enabled UAV Network Model.

TABLE I
NOTATION/ABBREVIATION/ACRONYM AND ITS DEFINITION.

Notation / Abbreviation / Acronym	Definition
UAV-BS	UAV-Base station
VLC	Visible Light Communication
UB_v	VLC enabled UAV-BS
UB_r	RF enabled UAV-BS
RGB	Red, green and blue
LSD	Light Shaping Diffuser
ES	Exhaustive search based strategy
FU	Farthest user based strategy
SU	Shifting UAV based strategy
R	Maximum coverage radius
L_o	Optimal altitude
SNR_{th}	Signal-to-noise ratio threshold
E_{th}	Illuminance threshold
P_{th}	Transmitted optical power
U_e	Average number of effective users covered
$\mathcal{S}$	Average service time

of UB_v is considered as 'T' seconds to serve N ground users. The users are moving around following a random walk mobility model. The communication network decides UB_v altitude (L) and its maximum coverage radius (R) as shown in Fig. 1 based on two QoS metrics: desired illuminance and reliable communication. The reliable communication metric is decided based on the SNR at the edge of the coverage area. Therefore, reliable communication and SNR has been used interchangeably in this paper. This work considers illuminance (in Lux) and SNR (in dB) at forward error correction (FEC) limit bit-error-rate (BER). Further, UB_v does not require to serve as an illuminaire for day scenarios assuming daylight is enough for visibility, so only SNR QoS metric has been considered in the day scenario. However, for night scenarios, UB_v can simultaneously communicate with users and illuminate the users' plane. Hence, both illuminance and SNR have been considered as QoS metrics in determining R and its corresponding optimum altitude $L_o = L$ in Fig. 1. Once L_o has been obtained, then we focus on the x-y axes (i.e., 2-D) placement of UB_v in the horizontal plane. In the following subsections, we introduce the two QoS metrics.

A. SNR in VLC channel

The received SNR [28], [29] at the ground users' plane can be defined as

$$\mathrm{SNR} = \frac{[\rho H(0) P_t]^2}{N_o B}, \tag{1}$$

where, ρ is the responsivity of the photodetector (PD), P_t is the transmitted optical power of LED, B is the VLC channel bandwidth, N_o is the noise power spectral density (PSD) of additive white Gaussian noise (AWGN) with zero mean generated at PD. It has been assumed that the impact of ambient light noise can be removed with a high pass filter [3], [8]. $H(0)$ is the channel gain of the dominant line-of-sight (LOS) component of the VLC channel. The $\mathrm{UB_v}$ can serve users indoor and outdoor both. However, we have considered outdoor scenarios without atmospheric turbulence in this work for simplicity. $\mathrm{UB_v}$ serve users at an open area, so there will be less possibility of strong reflections from outdoor buildings and infrastructures, hence only the dominant component i.e., LOS link of the optical channel [8], [9] has been considered. $H(0)$ can be obtained from radiation intensity pattern [28], [29] given as:

$$H(0) = \begin{cases} \frac{(m+1)A}{2\pi D_d^2} \cos^m(\phi) T_s(\psi) g(\psi) \cos(\psi), & 0 \le \psi \le \psi_c \\ 0, & \psi > \psi_c \end{cases} \tag{2}$$

where, A is the physical area of the PD, ϕ is the angle of irradiance, ψ is the angle of incidence at the PD which should not exceed the field-of-view (FOV) angle (ψ_c) of the PD for proper data reception ($0 \le \psi \le \psi_c$). The Euclidean distance (D_d) between the $\mathrm{UB_v}$ (VLC transmitter) and the ground user (VLC receiver) is equal to $\sqrt{L^2 + r^2}$ as inferred from Fig. 1. With zero elevation and orientation of the users, the angle of incidence becomes equal to the angle of irradiance [30], [31]. Hence, the term $\cos(\phi)$ and $\cos(\psi)$ become equal to $\frac{L}{D_d}$. The order of Lambertian emission is denoted by m and is determined by $\phi_{\frac{1}{2}}$, semi-angle at half illuminance of an LED as:

$$m = \frac{-\ln(2)}{\ln(\cos(\phi_{\frac{1}{2}}))} \quad . \tag{3}$$

In (2), $T_s(\psi)$ is the gain of the optical filter, and $g(\psi)$ is the gain of the optical concentrator given as:

$$g(\psi) = \frac{n^2}{\sin^2(\psi_c)}, \qquad 0 \le \psi \le \psi_c \tag{4}$$

where, n is the refractive index of optical concentrator. We compute the SNR required to fulfill the QoS metric by utilizing (1)-(4) to plot BER versus the SNR curve. The SNR threshold (SNR_{th}) is the minimum average received SNR required at the LOS user end for reliable communication at FEC limit BER with on-off keying (OOK) modulation scheme comes out to be around 13 dB in the VLC channel. Therefore, $SNR_{th} =$ 13 dB has been considered for the final maximum coverage radius and optimal altitude (L_o) calculation.

B. Illuminance

Illuminance is the amount of light falling over a given surface area which correlates with how humans perceive the brightness of an illuminated area [32], [33]. The unit of illuminance is "lux," where one lux is defined as the illuminance at which one-lumen luminous flux is uniformly radiated to 1 m^2 area. The amount of light landing on the users' plane (horizontal surface) is determined by

$$E = \frac{I(0) \cos^m(\phi)}{D_d^2}, \qquad -\pi/2 \le \phi \le \pi/2 \tag{5}$$

where $I(0)$ is the central luminous intensity of an LED.

The commercial LED follows the Lambertian radiation pattern. Thus, the radiant intensity $R_I(\phi)$ and luminous intensity $I(\phi)$ both depend on the angle of irradiance [28], [32], [33]. The relation between $I(\phi)$ and $R_I(\phi)$ has to be taken into account to obtain $I(0)$ in terms of $R_I(0)$ (central radiant intensity) and then finally in terms of P_t as expressed in (6). The SNR and illuminance of the ground users are obtained for a particular P_t which is then compared to their respective threshold value in order to check if it fulfills the desired QoS.

$$\begin{aligned} R_I(\phi) &= \frac{(m+1)P_t}{2\pi} \cos^m(\phi), \\ R_I(0) &= \frac{(m+1)P_t}{2\pi}. \end{aligned} \tag{6}$$

The requirement of $\mathrm{UB_v}$ to serve as a luminaire is important for night scenarios for safety and visibility purposes, since during daytime sunlight is enough for outdoor scenarios. Hence, $I(0)$ has been calculated as per humans' sensitivity to low light conditions.

$$\begin{aligned} I(0) &= (1700) R_I(0) V_\lambda, \\ I(0) &= \frac{(1700)(m+1) P_t V_\lambda}{2\pi}, \end{aligned} \tag{7}$$

where, the value 1700 in lumens/watt is based upon the sensitivity of the eye at 507 nm, the peak efficiency of the night (scotopic) vision curve and V_λ is the luminous efficacy of the eye. It is noted that the luminous intensity is the part of the optical intensity which is perceived as light by the human eye. Further, the response of the eye as a function of frequency is known as the luminous efficacy of the eye. The V_λ and its converted value in lumens/watt has been tabulated for both the day scenario (photopic) case and the night scenario (scotopic) case in [34]. Therefore, for the dark-adapted (scotopic) case, V_λ is one at 507 nm. Similarly for photopic case, V_λ is one at 555 nm which is 683 lumens/watt [34]. Therefore, $I(0)$ varies for day and night scenarios and depends on the dominant light frequency. This in turn varies E, and thus E should be calculated specifically for day and night scenarios.

As stated earlier, illumination from $\mathrm{UB_v}$ is usually meant for night safety along with sustainable street lighting. In [35], the recommended levels of illumination required have been tabulated for different road characteristics to maintain visibility for safety purposes as per the World Bank report for Indian streets. Therefore, in our work, we have considered the scenario nearby secondary roads [35], hence E_{th} is fixed to 4 Lux as QoS metric to obtain R and L_o. Nevertheless, the illuminance threshold can not only be specific to Indian road scenarios; it can be decided as per the applications (such as environmental protection monitoring) and its requirements.

III. Problem Formulation and Solution

The problem is to optimize the 3-D UB_v placement and update interval while maintaining the desired threshold of illuminance and SNR. Specifically, we determine the coverage radius of UB_v and its optimal altitude based on the predefined QoS metrics. Assuming that the minimum illuminance and SNR requirement does not change during T, the optimal altitude can be fixed during T. However, there is a possibility that UB_v may not cover all the ground users at a particular time instant due to their random mobility and fixed R. Consequently, UB_v 2-D placement needs to be updated after certain time intervals. It may be noted that the altitude optimization can be decoupled from the 2-D UB_v placement updates which occur more frequently. Therefore, the optimization of 3-D placements of UB_v is divided into two problems- where the placement in the z-axis (altitude) is done first and then x-y axes placement is updated from time to time based on the user mobility. Nevertheless, even in the case of non-flat areas, the altitude placement can be updated as per users' elevation with respect to the lowest elevation as a reference. However, the update time for altitude placement would be larger than x-y placement due to users' less frequent displacement in the z-axis. In this work, we have assumed that if there is elevation at the user's plane, then after total flight time (T), the altitude can be updated once. In the following sections, we discuss UB_v optimal altitude first and then joint optimization of 2-D UB_v placement and update interval.

A. Optimal Altitude

The altitude (L) placement of UB_v should provide the maximum possible coverage radius (R) at the users' plane. The coverage radius (r) can be expressed in terms of L and other parameters known to us from SNR and illuminance equation (as shown in (1) and (5)). The expressions of coverage radius in terms of L, E_{th} and SNR_{th} are as follows:

$$r_{SNR} = \sqrt{(\Upsilon^{\frac{1}{m+3}} - L^2)},$$
$$\Upsilon = \frac{\left[\rho P_t (m+1) A \cos^m(\phi) T_s(\psi) g(\psi) \cos(\psi) L^{m+1}\right]^2}{4\pi^2 SNR_{th} N_o B}, \tag{8}$$

$$r_E = \sqrt{\left[\left(\frac{(1700) V_\lambda \rho P_t L^m}{\pi E_{th}}\right)^{\frac{2}{m+2}} - L^2\right]}. \tag{9}$$

The second-order derivative of r_{SNR} and r_E are obtained to get the optimum values of L, respectively. Thus, the optimized altitude (L_o^{SNR}) obtained from r_{SNR} is used to calculate R for SNR QoS, whereas L_o^E obtained from r_E is used to calculate R for illuminance QoS. The minimum of $[r_{SNR}(L_o^{SNR}), r_E(L_o^E)]$ obtained from (8) and (9), respectively, provides final R which satisfies both illuminance and communication. The R and coverage area thus obtained gets limited due to the QoS constraints. The most common way to increase R is by increasing the altitude of UB_v. However, with increasing height, the VLC channel gain (refer (2)) reduces, as it is inversely proportional to the square of the distance between transmitter and receiver (in our case, the distance is the altitude of UB_v from the ground users). Hence, for reliable communication at the ground users, the transmitted optical power can be increased [19], thereby increasing the received power. However, increasing power is not an energy-aware choice, especially when the focus is on the energy-aware deployment of resource-constrained devices such as UAVs. Further, many recent papers have increased the reliable communication distance between VLC transmitter and receiver to a hundred meters in an outdoor scenario [36]–[38]. Nevertheless, these techniques will alleviate the issue of reliable communication at high altitudes of UB_v, but with additional energy and hardware cost. In this work, the coverage area of UB_v has been enhanced with energy-aware techniques complying with the greener aspect of communication.

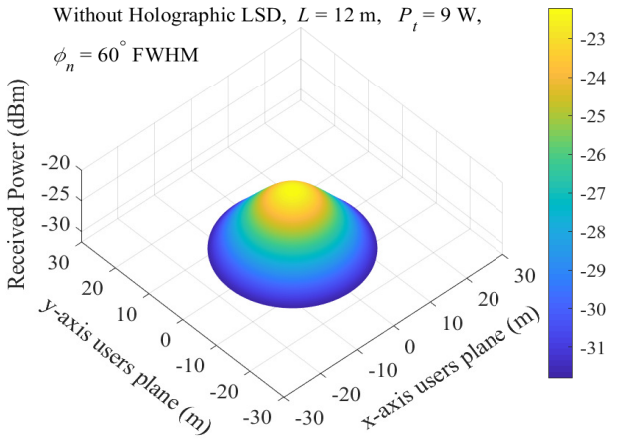

Fig. 2. Received power distribution in the coverage area without holographic LSD.

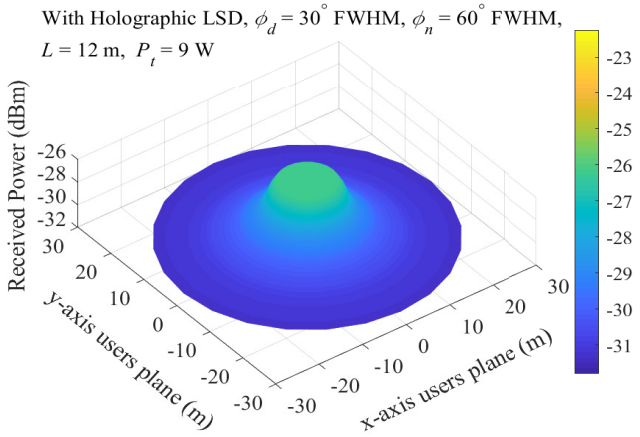

Fig. 3. Received power distribution in the coverage area with holographic LSD.

1) holographic LSD: Holographic LSDs of different angles are employed to increase the coverage area of an LED with uniform power distribution [24], [25]. In order to ensure larger coverage and optimum link performance, holographic shaping lenses can be used at the transmitter. Using holographic LSD, the effective divergence angle of the transmitter LED can be extended to

$$\phi_e = \sqrt{\phi_n + \phi_d}, \tag{10}$$

where ϕ_e is the effective output angle of the light, ϕ_n is the irradiance angle of the LED in full width half maximum

(FWHM), and ϕ_d is the viewing angle of LSD. The calculation of beam intensity through holographic LSD has been simplified in Fig. 4 of [25], where LSD is divided into an array of pixels, and the beam profile for every pixel follows the VLC channel. The light intensity can be considered uniform for a very tiny beam profile after passing through a single pixel. Finally, the effective coverage radius by a transmitter LED at an altitude of L utilizing LSD at its front head can be obtained as follows:

$$r_{LSD} = L\tan(\phi_e). \tag{11}$$

The coverage area now depends on the increased coverage radius, r_{LSD}. Further, with the utilization of LSD, the received power distribution at the coverage area becomes more uniformly distributed, which can be observed from Figs. 2 and 3. The received optical power becomes the average of the sum of individual footprints per pixel.

2) RGB LED: The central luminous intensity of an LED depends on V_λ. At 507 nm, $V_\lambda = 1$ and 1700 lumens/watt is sensed by the human eye [34], which is highest for scotopic case. It is difficult to design the peak wavelength of a yellow phosphorus-based LED at 507 nm or close to 507 nm to get higher illuminance with radiated light as white light. However, RGB LEDs can be designed for certain dominant wavelengths while maintaining white light [39]. The combined effect of red, green and blue light wavelengths can be utilized to obtain the value of V_λ as close as possible to one, which in turn will increase the illuminance. The central wavelength of RGB LEDs and its coordinates from the CIE 1931 color space [40] are shown in Table II. The luminous efficacy of red (V_λ^r), green (V_λ^r) and blue (V_λ^r) wavelengths are 0.001497, 0.811 and 0.676, respectively [34]. The optical power of different wavelengths can be adjusted such that it increases the overall luminous efficacy. The overall luminous efficacy of RGB LED can be expressed as:

TABLE II
THE CORRESPONDING COORDINATES OF CENTRAL WAVELENGTHS OF RGB LEDS IN CIE 1931 COLOR SPACE.

LED light color	Wavelength	Coordinates x	Coordinates y
Red	640 nm	0.7190	0.2809
Green	530 nm	0.1547	0.8059
Blue	465 nm	0.1355	0.0399

$$V_\lambda^{rgb} = (1700)V_\lambda^r P_r + (1700)V_\lambda^g P_g + (1700)V_\lambda^b P_b, \quad P_r + P_g + P_b = 1, \tag{12}$$

where, P_r, P_g and P_b are the normalized optical power of red, green and blue LEDs, respectively. Further, while increasing V_λ^{rgb}, the value of P_r, P_g and P_b should also maintain white tone light. The final x, y chromaticity coordinates of an RGB LED must fall inside the white region of CIE 1931 chromaticity diagram so as to emit white colour light [39]. The relation between P_r, P_g, P_b and x, y chromaticity coordinates is shown below:

$$\begin{aligned} x &= x_r \cdot P_r + x_g \cdot P_g + x_b \cdot P_b, \\ y &= y_r \cdot P_r + y_g \cdot P_g + y_b \cdot P_b, \end{aligned} \tag{13}$$

where the coordinates of central wavelength of red LED light is (x_r, y_r), green LED light is (x_g, y_g) and blue LED light is (x_b, y_b) in the CIE chromaticity color space. (13) can be re-written using coordinate values from Table II as:

$$\begin{aligned} x &= 0.7190 \cdot P_r + 0.1547 \cdot P_g + 0.1355 \cdot P_b, \\ y &= 0.2809 \cdot P_r + 0.8059 \cdot P_g + 0.0399 \cdot P_b. \end{aligned} \tag{14}$$

Using (12) and (14), the possible values of P_r, P_g and P_b are obtained which increases V_λ^{rgb} while satisfying the white tone light constraint. $P_r = 0.15$, $P_g = 0.3$ and $P_b = 0.55$ have been considered in this work. Therefore, while calculating r_E for scotopic case utilizing RGB LED based solution, the V_λ in (9) is replaced with V_λ^{rgb} as shown in (12).

B. Analytical Solution for Optimum Coverage Radius

The analytical solution for optimum coverage radius with the proposed RGB LED and holographic LSD utilizes (15) and (16), which have been derived using (8) and (9), as fundamental equations for illuminance and SNR QoS metrics, respectively. Therefore, the r_E and r_{SNR} (as shown in (9) and (8)) must incorporate the effect of holographic LSD and RGB LED concept to analytically obtain the maximum coverage radius which satisfies both illuminance and communication. The modified expressions of coverage radius incorporating the effect of holographic LSD and RGB LED concept are as follows:

$$\begin{aligned} r_{SNR}^{'} &= \sqrt{(\Upsilon^{'\frac{1}{m'+3}} - L^2)}, \\ \Upsilon^{'} &= \frac{\left[\rho P_t \xi_{SNR}(m'+1)A\cos^{m'}(\phi_e)\chi L^{m'+1}\right]^2}{4\pi^2 SNR_{th} N_o B}, \\ \chi &= T_s(\psi)g(\psi)\cos(\psi), \end{aligned} \tag{15}$$

$$r_E^{'} = \sqrt{\left[\left(\frac{(1700)V_\lambda^{rgb}\rho P_t \xi_E L^{m'}}{\pi E_{th}}\right)^{\frac{2}{m'+2}} - L^2\right]}, \tag{16}$$

While using holographic LSD, the effective divergence angle of the transmitter LED (ϕ_e) should be considered for calculating Lambertian order. Therefore, instead of conventional Lambertian order (m) in (8) and (9), modified Lambertian order ($m' = \frac{-\ln(2)}{\ln(\cos(\phi_e))}$) has been used in (15) and (16). LEDs, with no shaping lenses, behave as a Lambertian source. However, the holographic LSD changes the intensity pattern, which in turn changes the received SNR distribution (as seen in Fig. 3). Since we have derived the expressions ((15) and (16)) based on conventional intensity pattern in (8) and (9). Therefore, the transmitted power is adjusted with a factor of ξ_{SNR} and ξ_E, in (16) and (15), respectively, to incorporate the changes in intensity pattern due to holographic LSD. The factor $\xi_{SNR} = \frac{P_r^{LSD}}{P_r}$, where, P_r^{LSD} and P_r are the optical power received at the circumference of coverage area for particular L with and without holographic LSD, respectively. Similarly, the factor $\xi_E = \frac{E_r^{LSD}}{E_r}$, where, E_r^{LSD} and E_r are the illuminance received at the circumference of coverage area for particular L with and without holographic LSD, respectively. Further, the V_λ of LED changes as per the RGB LED concept.

Thus, the overall luminous efficacy of RGB LED (V_λ^{rgb}) as obtained from (12) is considered in (15).

The second-order differentiation of (15) and (16) is derived to obtain the maximum value of altitude L_o^E and L_o^{SNR}, respectively. The respective altitude values are used in (15) and (16) to obtain respective coverage radius. Further, with the use of holographic LSD, the direct impact is the increased coverage radius (as seen in Figs. 2 and 3), so when the QoS metrics are satisfied till a certain UB_v altitude, the r_{LSD} limits the R. Therefore, r_{LSD} calculated from (11) for L_o^E and L_o^{SNR}) has been considered in (17).

$$R = \min \ \left[\ r_E^{'}(L_o^E), \ \ r_{SNR}^{'}(L_o^{SNR}), \ r_{LSD}(L_o^E), \ \ r_{LSD}(L_o^{SNR}) \ \right], \tag{17}$$

The maximum coverage radius, as seen in (17), can be obtained by finding the minimum of different optimized r as per the required QoS metrics. Therefore, a network engineer can directly deduce the maximum coverage radius and its optimum altitude utilizing the proposed novel analytical expressions ((15) and (16)) at a given QoS metric for the proposed RGB LED and holographic LSD technique.

C. Joint Optimization of 2-D Placement and Update Interval

Fig. 4 illustrates the UB_v placement update timeline for total operational time, T seconds. The time at which UB_v 2-D positioning is updated, is termed as an update instant. The time difference between two consecutive update instants (k and $k+1$) is denoted as the update interval $t_{up}(k)$. After optimizing the altitude of UB_v in terms of maximum coverage radius, the proposed work in this paper optimizes the x-y placement of UB_v in order to maximize the number of users covered subject to the fairness of coverage. The coordinates of the projection of

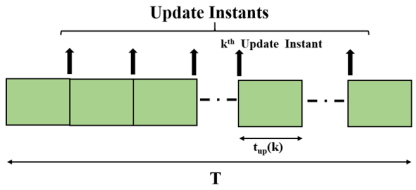

Fig. 4. UB_v placement timeline.

UB_v in the 2-D user plane at the k^{th} update instant is denoted as $[U_\text{x}(k), U_\text{y}(k)]$. We require an indicator variable $G_n(k)$ to represent users coverage, when user n is covered at the update instant k, $G_n(k) = 1$ otherwise $G_n(k) = 0$. It should be noted that during $t_{up}(k)$ update interval the user's coverage indicator varies due to user's mobility between k^{th} and $(k+1)^{th}$ update instants. Hence, the coverage probability of user n at k^{th} update instant for $t_{up}(k)$ (denoted by $P_{n,t_{up}(k)}$) should be considered to obtain the effective number of users covered in an update interval. Therefore, the average number of effective users covered in l^{th} UB_v operation period is determined by $G_{n,k}$ and $P_{n,t_{up}(k)}$ as follows:

$$\bar{U_e} = \mathop{\mathbb{E}}_{l}\left[\frac{1}{K_l}\sum_{k=1}^{K_l}\sum_{n=1}^{N} G_{n,k}(k) P_{n,t_{up}(k)}\right], \\ = \mathop{\mathbb{E}}_{l}\left[E_{cov}(l)\right], \tag{18}$$

where $\mathbb{E}[.]$ is the expectation operator and N is the total number of mobile users considered. K_l denotes the number of update instants in l^{th} UB_v operation period. The number of effective users covered in l^{th} UB_v operation period is termed as $E_{cov}(l)$ in (18).

Further, maintaining the coverage fairness of mobile users become important, since there may be possibility of same set of users being covered more often than the other users [19]. According to Jain's fairness index [41], the fairness for the overall network at update instant k is defined as follows:

$$fair(k) = \frac{\left(\sum_{n=1}^{N}\sum_{i=0}^{i=k} G_n(i)\right)^2}{N\left(\sum_{n=1}^{N}\left(\sum_{i=0}^{i=k} G_n(i)\right)^2\right)}, \tag{19}$$

where i variable denotes the range of update instants.

The fly-hover communication protocol for UAV operation [42] suggest that UAVs serve users for communication only when it is in the hovering mode. Therefore, considering the fly-hover protocol in this work, at every update instants we require the time taken ($F(k)$) by the UB_v to fly to its new 2-D location with velocity v_U, as expressed in (20)). The UB_v hovering time is equivalent to its service time. The service time ($\mathcal{S}$) of UB_v out of total operation time T can be estimated from $F(k)$ in (21).

$$F(k) = \frac{1}{v_U}\sqrt{(U_\text{x}(k) - U_\text{x}(k-1))^2 + (U_\text{y}(k) - U_\text{y}(k-1))^2}, \tag{20}$$

$$\mathcal{S} = T - \mathop{\mathbb{E}}_{l}\left[\sum_{k=1}^{K_l} F(k)\right]. \tag{21}$$

The optimal UB_v placement problem at k^{th} update instant can be formulated as follows:

$$\begin{aligned} \text{P1:} \quad & \max \sum_{n=1}^{N} G_n(k) \\ \text{s.t.} \quad & \text{C1: } fair(k) > fair_{thres}, \\ & \text{C2: } F(k) < t_{up}(k). \end{aligned} \tag{22}$$

Here, the P1 objective function maximizes the total number of users covered at update instant k subject to constraints C1 and C2. C1 puts a lower bound on fairness with a threshold of $fair_{thres} \in [0, 1]$ in the network. In contrast, C2 puts an upper bound on $F(k)$ to ensure non-zero service time during the upcoming $t_{up}(k)$ seconds, hence $F(k)$ must be less than $t_{up}(k)$. The optimization problem, in this case, falls under the fair maximum coverage (FMC) type of problem [43]. Let's assume the considered hovering area (just above the user's plane at a certain altitude) as a complete graph and the possible hovering points as vertices. The paths to the hovering points are edges. The optimization problem reduces to Traveling Purchaser Problem (TPP). Further, with relaxed constraints, the optimization problem imitates the classical Traveling Salesman Problem (TSP) [44]. TSP and thus TPP are NP-hard, making the optimization problem (22) NP-hard as well [19]. Therefore, the FMC optimization problem of this work becomes difficult to be solved directly using traditional optimization techniques. The first approach to solve FMC problems is to go for an exhaustive search-based strategy

(ES) to obtain the best possible performance results, which is considered a benchmark for other optimization methods. One of the state-of-the-art optimization algorithms for FMC is the greedy approximation algorithm [15], [43], where one picks the hovering point of UB_v that covers the maximum number of users. ES method integrates the greedy approximation method in its algorithm. For a given $t_{up}(k)$, P1 has been solved with the exhaustive search-based strategy [14] as shown in Algorithm 1. ES method depends on the number of hovering points considered. A larger number of hovering points provide higher accuracy but with increased time complexity. Therefore, in order to achieve energy-aware deployment of UB_v, two energy-aware solutions are proposed to solve P1.

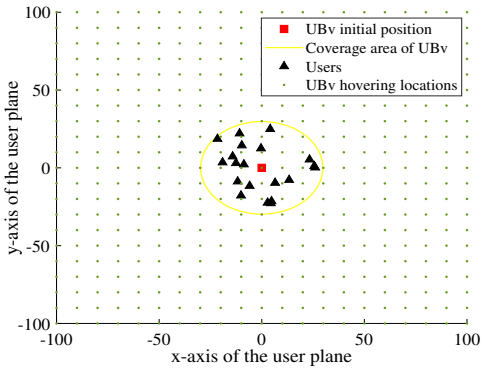

Fig. 5. ES method illustrating exhaustive-search strategy to determine optimal hovering point.

In Algorithm 1, $U_x^*(k-1)$ and $U_y^*(k-1)$ are the optimal coordinates at the $(k-1)^{th}$ update instant. At $k=1$, $t_{up}(1)$ is initialized as t_{min}. For $k>1$, $t_{up}(k)$ is initialized as $t_{up}^*(k-1)$ where, $t_{up}^*(k-1)$ is the optimal update interval at the $(k-1)^{th}$ update instant. Moreover, we consider that the 2-D hovering space of UB_v is discretized with a resolution of 10 m along the horizontal axis, as shown in Fig. 5. In Algorithm 1, Cov_{prev} is a list of $(k-1)$ vectors of length N, where an element in a vector will be '1' if user is covered otherwise '0'. For each of the hovering locations in Hov_{loc} (as represented by dots in Fig. 5), function `Cov ()` determines which of the N users may get covered. In case of ES method, Algorithm 1 considers Hov_{loc}. `Cov ()` assigns '1' if a user is covered else '0'. The output of `Cov ()` is stored in Cov_{mat}. Then, the flight time of the UB_v is computed using function `Fly ()`. Further, the fairness value corresponding to each hovering location is computed using `Fair ()` and stored in $Fairness$. Finally, inspired from the greedy approximate approach [15], function `Find ()` outputs $U_x(k)$, $U_y(k)$ that maximize the number of users covered while satisfying the constraints C1 and C2. Also, we obtain the values of $G_n(k)\ \forall\, n$.

The optimization problem can be approached as a combinatorial problem since all the possible hovering points (vertices in a graph) are potential candidates for optimum hovering point. The ES method to solve P1 is a time-consuming and computationally extensive process because it searches all the hovering locations of the user's plane to maximize the total number of users covered. For energy-constrained rotary UAVs, this work aims to propose energy-aware solutions to position UB_v. Space reduction method (SRM) [45] is a state-of-the-art

Algorithm 1: Exhaustive / Farthest user based solution to P1 at k^{th} update instant.

Input: $t_{up}(k)$, $U_x^*(k-1)$, $U_y^*(k-1)$, $fair_{thres}$
$\mathcal{X}$ - List of x coordinates of N users at k^{th} update instant
$\mathcal{Y}$ - List of y coordinates of N users at k^{th} update instant
Hov_{loc} - List of 2-D UB_v Hovering locations
$Hov'_{loc}(k)$ - List of 2-D UB_v Hovering locations till the farthest user at k^{th} update instant
Cov_{prev} - List of vectors containing coverage information of all users till $(k-1)^{th}$ update instant
Output: $\mathcal{G}$ - List of $G_n(k)\ \forall\, n$, $U_x(k)$, $U_y(k)$
Initialize: $Cov_{mat}=\emptyset$, $Fly_{time}=\emptyset$, $Fairness=\emptyset$
for $s=1:1:|Hov_{loc}|/|Hov'_{loc}(k)|$ **do**
  $Cov_{mat}(:,s)$ = `Cov`($\mathcal{X}$, $\mathcal{Y}$, $Hov_{loc}/|Hov'_{loc}(k)|$)
  $Fly_{time}(s)$ = `Fly` (($U_x^*(k-1)$, $U_y^*(k-1)$, $Hov_{loc}/|Hov'_{loc}(k)|$)
  $Fairness(s)$ = `Fair`(Cov_{mat}, Cov_{prev}),
end for
[$U_x(k)$, $U_y(k)$, $Index1$]=`Find`($Cov_{mat}, Fairness, Fly_{time}, fair_{thres}, t_{up}(k)$),
$Cov_{prev}(:,k)=Cov_{mat}(:,Index1)$,
$\mathcal{G}=Cov_{mat}(:,Index1)$

approach where the search space is reduced without losing optimal solution. SRM is particularly applicable to searching graphs with vertices and edges. Therefore, instead of searching all hovering points, the hovering points until the farthest user are searched at an update instant. For farthest user-based (FU) method, all the hovering points under the purple circle as shown in Fig. 6 is considered in the search space of k^{th} update instant to obtain optimal UB_v hovering point. It undoubtedly reduces the search space. However, it is interesting to explore how the performance metrics such as $\bar{U}_e$ and $\mathcal{S}$ behave in the UB_v network with the FU method.

The algorithm to solve P1 by FU method follows the same steps of Algorithm 1 with same notations except Hov_{loc}. The difference between ES and FU method lies in considering the 2-D hovering space of UB_v. In Algorithm 1, Hov_{loc} is replaced by $Hov'_{loc}(k)$ for FU method. At k^{th} update instant, the mean location ($[\bar{x}(k), \bar{y}(k)]$) of all the users is calculated. The distance of the farthest user from the mean location is obtained, which forms the radius of the circle with $[\bar{x}(k), \bar{y}(k)]$ as the centre x-y points for calculating $Hov'_{loc}(k)$. For example, let's assume that the user's location at k^{th} update instant is as per Fig. 6, so all the hovering points from the list of Hov_{loc} falling inside the purple circle represents $Hov'_{loc}(k)$. Finally, P1 is solved for all the K_l update instants in l^{th} UB_v operation period.

With FU method, it is observed from Algorithm 1 that the range of s reduces ($Hov'_{loc}(k) < Hov_{loc}$). However, the FU method still depends on the list of hovering locations. Therefore, in shifting UAV (SU) strategy, as illustrated in Fig. 7, we try to eliminate the dependency on the list of hovering locations by considering the user's location to decide the optimal UB_v placement. SU method is influenced by the random shifting technique [46], [47]. However, in our case we deterministically use the shifting method so as to get the optimum hovering point of UB_v within flight time. At k^{th} update instant, some users are covered by the UB_v for communication, whereas others are not, so let's call them uncovered users (U_{uncov}). As network fairness or covered users decreases beyond a threshold at k^{th} update instant, the

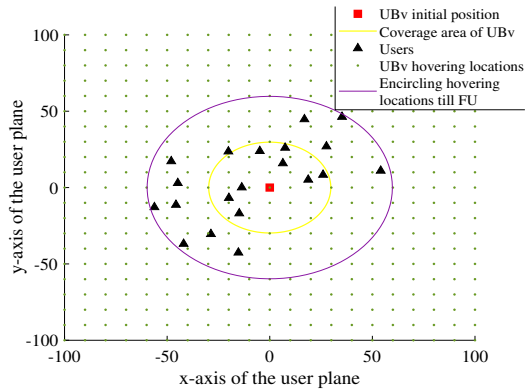

Fig. 6. FU method illustrating farthest user strategy to determine optimal hovering point.

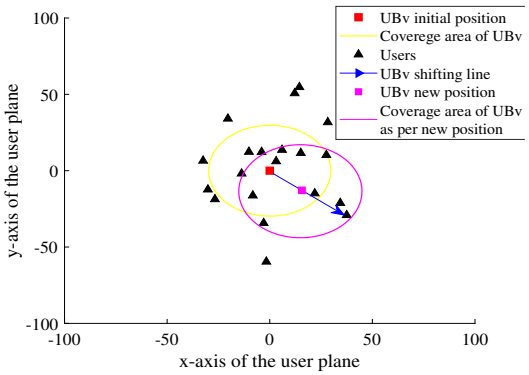

Fig. 7. SU method illustrating shifting UAV strategy to determine optimal hovering point.

UB_v shifts its position as per the previous coverage probability and closeness of U_{uncov} from UB_v's $(k-1)^{th}$ location to cover a maximum number of users while maintaining the constraints C1 and C2.

In Algorithm 2, U_{cov} and U_{uncov}, denotes the number of covered and uncovered users, at k^{th} update instant, respectively. At k^{th} update instant; if $Fairness$ and U_{cov} are greater than its respective threshold, then the UB_v placement is kept the same as the $(k-1)^{th}$ update instant. However, the UB_v position is shifted whenever the above criteria do not hold for a given update instant. The function `Shift ()` utilizes the list of $\mathcal{X}'$ and $\mathcal{Y}'$ coordinates and Cov_{prev} to calculate new possible positions of UB_v as per each uncovered users. The possible shifted positions are stored in $U'_x(s)$ and $U'_y(s)$ for all U_{cov} at the $(k-1)^{th}$ update instant. The function `Find ()` outputs the index out of range s, maximizing the number of users covered while satisfying C1 and C2. Finally, the index obtained from `Find ()` is utilized to get optimal UB_v placement.

After solving P1 with three different algorithms to get $\mathcal{G}$, the next problem is to find the optimal value of $t_{up}(k)$. The choice of $t_{up}(k)$ depends on two factors: 1) temporal user coverage probability and 2) total UAV flight time. For visual clarity, Figs. 8 and 9 have been shown to depict the behaviour of above mentioned two factors with $t_{up}(k)$. The random distances covered by each mobile user in each transition follows a random walk mobility model and is presumed to be Rayleigh distributed random variable with parameter σ. Interestingly, a network engineer would require higher temporal user coverage probability and lower total UAV flight time, hence there is a trade-off between these two factors. Additionally, as expressed in (21), an increase in the UB_v flight time decreases its service time. Hence, minimization of total UB_v flight time during T seconds must be considered when optimizing $t_{up}(k)$.

1) Temporal Coverage Probability: The coverage probability of a user must capture the change in user locations even over an update interval. Therefore, at the k^{th} update instant, the temporal coverage probability of covered user n is the probability of it being within UB_v coverage area for the upcoming $t_{up}(k)$ seconds. A user may have multiple transitions during these $t_{up}(k)$ seconds. The number of transitions depends on the random walk parameter, σ and the velocity of the users, v_u. In other words, temporal coverage probability can be defined as the probability, that the displacement of the user from UB_v must be less than R for all the transitions within $t_{up}(k)$. The temporal coverage probability metric proposed in [14] helps in establishing a relationship between user mobility and $t_{up}(k)$.

In Fig. 8, as $t_{up}(k)$ increases, the effective number of users covered decreases because higher update interval corresponds to few UB_v placement updates and hence during that interval most of the mobile users come out of the coverage area. Since, the effective number of users covered is directly proportional to coverage probability as seen in (18). Therefore, $t_{up}(k)$ must be selected in such a manner that it maximizes the coverage probability. Further, while optimizing $t_{up}(k)$, the coverage probability of all the users covered at k^{th} instant must be considered.

Algorithm 2: Shifting UAV based solution to P1 at k^{th} update instant.

Input: $t_{up}(k)$, $U^*_\text{x}(k-1)$, $U^*_\text{y}(k-1)$, $fair_{thres}$
$\mathcal{X}$ - List of x coordinates of N users at k^{th} update instant
$\mathcal{Y}$ - List of y coordinates of N users at k^{th} update instant
Cov_{prev} - List of vectors containing coverage information of all users till $(k-1)^{th}$ update instant
U_{cov} - Number of covered users at k^{th} update instant
Output: $\mathcal{G}$ - List of $G_n(k)\ \forall\, n$, $U_\text{x}(k)$, $U_\text{y}(k)$
if $Fairness > fair_{thres}$ && $U_{cov} > 0.75N$ **then**
    $[U_\text{x}(k), U_\text{y}(k)] = [U^*_\text{x}(k-1), U^*_\text{y}(k-1)]$
    $Cov_{prev}(:,k) = Cov_{mat}(:,k)$,
    $\mathcal{G} = Cov_{mat}(:,k)$
end if
else
    $\mathcal{X}'$ - List of x coordinates of uncovered users at k^{th} update instant
    $\mathcal{Y}'$ - List of y coordinates of uncovered users at k^{th} update instant
    U_{uncov} - Number of uncovered users at k^{th} update instant
    Initialize: $Cov_{mat} = \emptyset$, $Fly_{time} = \emptyset$, $Fairness = \emptyset$
    for $s = 1:1:|U_{uncov}|$ **do**
        $S_x(s), S_y(s) = \texttt{Shift}(\mathcal{X}', \mathcal{Y}', Cov_{prev})$
        $[U'_x(s), U'_y(s)] = [U^*_\text{x}(k-1) + S_x(s), U^*_\text{y}(k-1) + S_y(s)]$
        $Cov_{mat}(:,s) = \texttt{Cov}(\mathcal{X}, \mathcal{Y}, U_\text{x}(s), U_\text{y}(s))$
        $Fly_{time}(s) = \texttt{Fly}\ (U^*_\text{x}(k-1), U^*_\text{y}(k-1), U_\text{x}(s), U_\text{y}(s))$
        $Fairness(s) = \texttt{Fair}(Cov_{mat}, Cov_{prev})$,
    end for
    $[Index1]$=$\texttt{Find}(Cov_{mat}, Fairness, Fly_{time}, fair_{thres}, t_{up}(k))$,
    $[U_\text{x}(k), U_\text{y}(k)] = [U'_x(Index1), U'_y(Index1)]$
    $Cov_{prev}(:,k) = Cov_{mat}(:,Index1)$,
    $\mathcal{G} = Cov_{mat}(:,Index1)$
end if

This article has been accepted for publication in a future issue of this journal, but has not been fully edited. Content may change prior to final publication. Citation information: DOI 10.1109/TGCN.2022.3171920, IEEE Transactions on Green Communications and Networking

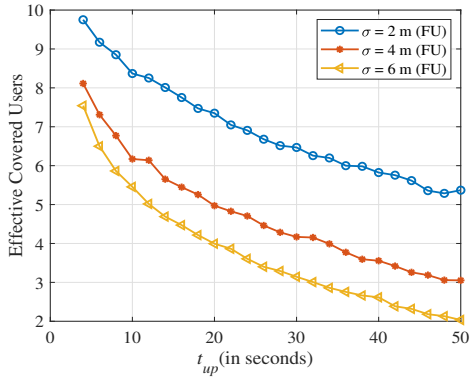

Fig. 8. Coverage probability of users for varying random walk parameter obtained on solving P1 with FU strategy versus update interval.

2) Total Flight Time: The average UB_v flight time during t_{up} will be $\mathbb{E}\left[F_{t_{up}}\right]$ and can be formulated as follows:

$$\mathbb{E}\left[F_{t_{up}}\right] = \frac{\mathbb{E}\left[\sum_{i=1}^{\frac{T}{t_{up}}-1} F(i)\right]}{\left(\frac{T}{t_{up}}\right)-1}, \tag{23}$$

where $\mathbb{E}\left[\sum_{i=1}^{\frac{T}{t_{up}}-1} F(i)\right]$ is the average total UB_v flight time when updates are done after every t_{up} seconds. First, the term $\sum_{i=1}^{\frac{T}{t_{up}}-1} F(i)$ can be determined in an offline manner by solving P1 for $\left(\frac{T}{t_{up}}-1\right)$ update instants. Consequently, $\mathbb{E}\left[\sum_{i=1}^{\frac{T}{t_{up}}-1} F(i)\right]$ is the average of the above summation. A typical plot of average total UB_v flight time has been shown in Fig. 9. It can be observed that as t_{up} increases the total UB_v flight time decreases. This is because lower update interval corresponds to frequent UB_v placement updates or vice versa. Consequently, the UB_v flies more frequently resulting in higher total UB_v flight time. Since there are

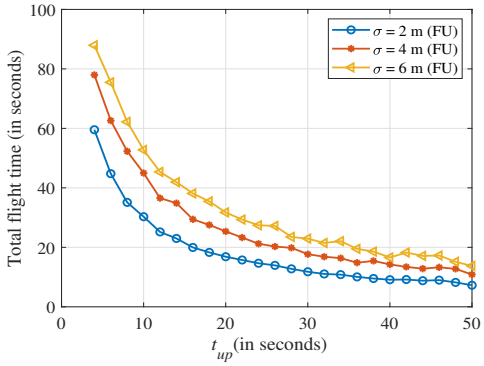

Fig. 9. Total UB_v flight time for varying σ obtained on solving P1 with FU strategy versus update interval.

two factors impacting the choice of $t_{up}(k)$, the first factor corresponds to the total flight time which is actually a fraction of T during which UB_v is in flight mode and cannot serve. Let $F_{t_{up}(k)}$ be the UB_v flight time during $t_{up}(k)$ with an average of $\mathbb{E}\left[F_{t_{up}(k)}\right]$ and $Q = \left\lceil \frac{T-\sum_{j=0}^{k-1} t_{up}(j)}{t_{up}(k)} \right\rceil$ denotes the number of updates that may occur when update interval is fixed as $t_{up}(k)$ until completion of total operation time T. Therefore, the first term in the objective function becomes $\frac{\left(\sum_{j=1}^{k-1} F(j)+Q\,\mathbb{E}\left[F_{t_{up}(k)}\right]\right)}{T}$. The term $\sum_{j=1}^{k-1} F(j)$ remains same for all $t_{up}(k)$, hence the first terms is reduced to $\frac{Q\,\mathbb{E}\left[F_{t_{up}(k)}\right]}{T}$. The second factor is the sum of the effective covered users. A weight of α and $(1-\alpha)$ has been assigned to the two terms, respectively to propose the minimization of a weighted single objective function. Hence, the optimization problem to obtain optimal $t_{up}(k)$ can be formulated as follows:

$$\begin{aligned} \text{P2:} \quad & \min \left(\frac{\alpha Q\,\mathbb{E}\left[F_{t_{up}(k)}\right]}{T} + \frac{(1-\alpha)}{\sum_{n=1}^{N} G_{n,k} P_{n,t_{up}(k)}} \right) \\ & \text{s.t.} \quad t_{min} \le t_{up}(k) \le t_{max}, \end{aligned} \tag{24}$$

where t_{min} and t_{max} is the lower and upper bound for $t_{up}(k)$. The weight parameter α can be tuned according to the network operator's requirement. For instance, if maximizing the coverage probability is the only requirement, the operator may set α as 0. However, if minimizing UB_v flight time is the only requirement, α may be set to 1.

Algorithm 3: Solution to P2 at k^{th} update instant.

Input: $\mathcal{G}$ - List of $G_n(k)\ \forall n$
t_{list} - List of update interval values,
Output: $t_{up}(k)$
Initialize: $r = 1$
for $t = t_{min} : 2 : t_{max}$ **do**
  $Factor(r) = \frac{\alpha Q\,\mathbb{E}[F_t]}{T} + \frac{(1-\alpha)}{\sum_{n=1}^{N} A_{n,k} P_{n,t}}$
  r=r+1
end for
$Index2 = \texttt{Min}(Factor)$
$t_{out}(k) = t_{list}(Index2)$

In Algorithm 3, the update interval range has been discretized with a resolution of 2 seconds. The objective function in (24) is computed for each discretized update interval, and the values obtained are stored in $Factor$. `Min` () finds the index of the minimum value in $Factor$. Finally, $t_{out}(k)$ is obtained.

The $G_n(k)$ values obtained from P1 are provided to P2. P2 is then solved using Algorithm 3 to obtain the update interval. The output of P2 is then fed back to P1. It goes on iteratively till the update interval value converges. In general, for the convergence of update interval, the condition $|t_{up}(k) - t_{out}(k)| < \epsilon$ must be met, where $t_{up}(k)$ and $t_{out}(k)$ are the input and output of P1 Algorithm and P2 Algorithm, respectively. ϵ is the error tolerance value. In this work, $\epsilon = 0$ has been considered. Further, the update interval converges to $t^*_{up}(k)$ within few iterations. The number of iterations depends on the choice of ϵ as well as the resolution of the update interval. With an increase in ϵ, number of iterations required for convergence will decrease. However, with an increase in resolution, the number of iterations required for convergence increases.

D. Time Complexity Analysis

The UAVs are energy-constrained devices, hence energy-efficient algorithms are preferred for the deployment of UB_v.

To demonstrate the energy efficiency of the proposed algorithms (i.e., FU and SU) over the ES algorithm, the energy complexity model of the algorithms [48], [49] should be obtained. In [48], the author proposes an energy complexity measure at circuitry level including energy E and time t in the form of the expression Et^2 to be used as the measure of the efficiency of a computation. Therefore, on adopting Et^2 and considering the energy required for any UB_v operation and processing as constant, the Et^2 term becomes a function of time only. Further, assuming the algorithms to be truly sequential, the most energy-efficient algorithms are also the most time-efficient since, in both cases, the aim is to minimize the number of steps. Thus, the relationship between energy efficiency and time efficiency becomes proportional. Therefore, the time complexity of the algorithm indicates its energy efficiency only.

The time complexity of a set of steps is considered as $O(1)$ if it doesn't contain a loop, recursion and call to any other non-constant time function [50]. ES method complexity mainly depends on the number of hovering locations, the number of mobile users, and the number of update intervals. Firstly, the complexity of solving P1 is determined by computing the complexity of Algorithm 1. In Algorithm 1, the complexity mainly depends on the number of times the '**for** loop' is executed, which depends on $|Hov_{loc}|$. Further, for overall complexity, one should consider the complexity of different functions inside the '**for** loop' from steps 8-12. $Cov()$ function in step 9 determines which of the N users is covered for all hovering locations, so the complexity order for step 9 is $O(N \times M_{ES})$, symbolizing $|Hov_{loc}|$ as time-dependent variable M_{ES}. The complexity order of step 10 is $O(M_{ES})$ which evaluate the flight time of UB_v using function $Fly()$. Step 11 evaluates the fairness value of the users corresponding to each hovering location with the complexity order of $O(N \times M_{ES})$. On considering the maximum value of complexity amongst steps 9, 10 and 11, i.e., $O(N \times M_{ES})$ and after execution of '**for** loop', the complexity becomes $O(M_{ES}^2 N)$. Step 13 computes the 2-D position of UB_v which maximizes the number of covered users using function $Find()$ with complexity order as $O(N \times M_{ES})$. Further, $O(1)$ is the complexity order for steps 14 and 15, so overall complexity for Algorithm 1 is $\max[O(M_{ES}^2 N), O(N \times M_{ES}), O(1), O(1)]$, which in turn results to $O(M_{ES}^2 N)$.

$$K = \frac{(t_{max} - t_{min})}{2} + 1, \tag{25}$$

Algorithm 3 is related to problem P2 solution, which depends on the output of P1 to obtain the optimum update interval. Complexity order for this case mainly depends upon the '**for** loop' which is executed for the total number of update intervals. Here t_{min} and t_{max} are the first and the last update instants. If we assume K as variable which represents the total number of update intervals (as shown in (25)), then the complexity order for P2 after execution of the '**for** loop' is $O(K)$. Therefore, the overall time complexity of ES method is $O(M_{ES}^2 N)$ + $O(K)$.

In case of FU method, the number of search space for UB_v is reduced. This is reflected by the term $|Hov_{loc}^{'}|$ in the '**for** loop' in Algorithm 1. Assuming $|Hov_{loc}^{'}|$ as time-dependent variable M_{FU}, the complexity order of Algorithm 1 is $O(M_{FU}^2 N)$. From above discussion, it can be interpreted that $|Hov_{loc}^{'}| < |Hov_{loc}|$. In our case, for the given specific simulation setup parameters (as stated in Table IV) the total number of hovering locations (M_{FU}) is reduced by approximately two times i.e $M_{FU} < \frac{M_{ES}}{2}$ and thus the overall complexity order becomes $O(\frac{M_{ES}^2 N}{4})$ + $O(K)$.

The number of times the '**for** loop' is executed in Algorithm 2 depends only on the number of uncovered users. Assuming $|U_{uncov}|$ as a time-dependent variable N_{SU}, which is always a fraction of N. Therefore, in the SU method, as per specific simulation setup parameters, the $|U_{uncov}|$ value is approximated to $0.75 * N$. Further, other steps in Algorithm 2 is of order $O(1)$ or less than and equal to $O(N)$ inside or outside the '**for** loop'. Thus, the overall complexity order becomes $O(N_{SU} N)$ + $O(K)$.

IV. Results and Discussions

This section presents and analyzes the relation between coverage radius and altitude of UB_v under different QoS metrics. The impact on the relation between r and L on utilizing RGB LEDs designed for scotopic case with and without holographic LSD have been presented. Further, the results pertaining to the iterative solution for jointly optimizing P1 and P2 have been discussed in detail.

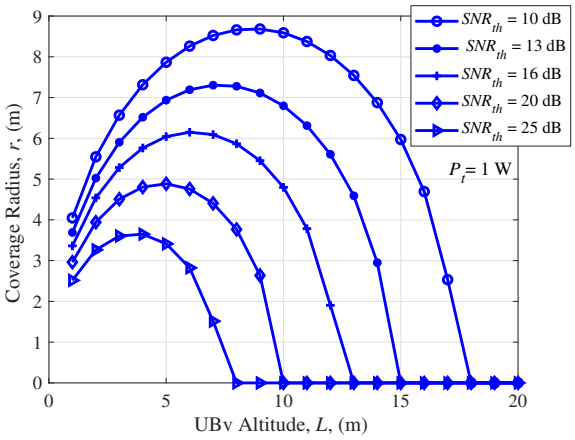

Fig. 10. Coverage radius versus altitude of UB_v for varying SNR thresholds at 1 W transmitted optical power.

Fig. 10 presents UB_v coverage radius with respect to its altitude at $P_t = 1$ W for different SNR threshold. It is observed that with increasing UB_v altitude, the coverage radius first increases and then decreases after reaching its peak value. Undoubtedly, with increasing altitude, the coverage of light increases as per (2). However, in this case, the aim is to cover users with a particular SNR threshold. Therefore, until a certain altitude, the coverage radius increases as it still fulfills the SNR threshold. However, the SNR threshold is responsible for decreasing the desired coverage radius after that.

In Fig. 11, the relation of UB_v coverage radius with its altitude have been shown for different illuminance threshold in day scenario (considering $V_\lambda = 1$ and maximum lumens/watt, i.e., 683 for photopic case) at transmitted optical power equal to one watt. It is observed that the illuminance threshold impacts the coverage radius and altitude range (defined as

This article has been accepted for publication in a future issue of this journal, but has not been fully edited. Content may change prior to final publication. Citation information: DOI 10.1109/TGCN.2022.3171920, IEEE Transactions on Green Communications and Networking

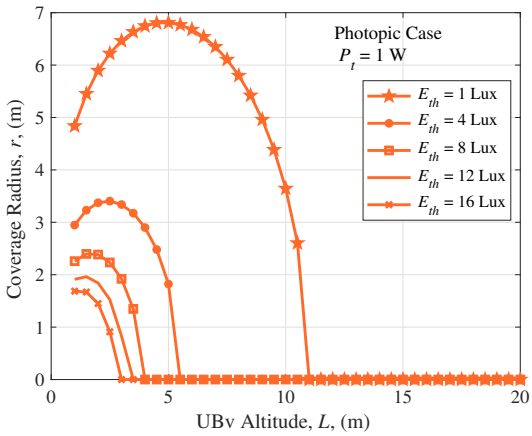

Fig. 11. Coverage radius versus altitude of UB_v of photopic designed RGB LED for varying illuminance threshold at 1 W transmitted optical power.

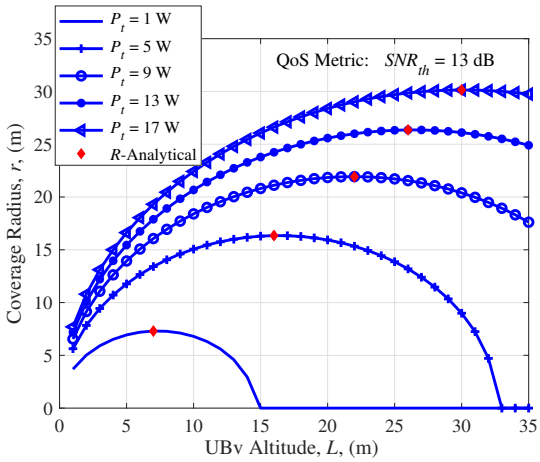

Fig. 13. Coverage radius versus altitude of UB_v for different transmitted optical power at 13 dB SNR threshold.

the highest altitude where coverage radius becomes zero) substantially as compared to the SNR threshold (in Fig. 10). The reason is due to the factor of light perceived by the human eye being considered in the illuminance expression (see (5) and (7)).

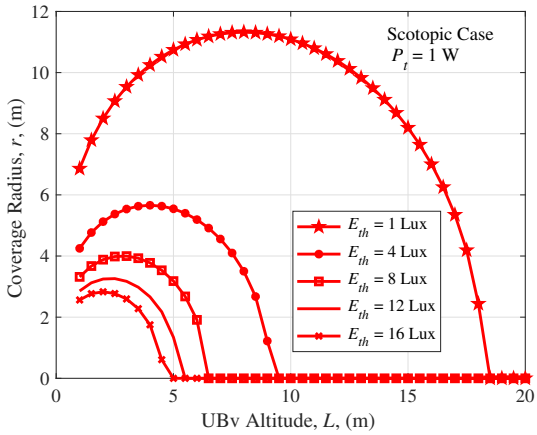

Fig. 12. Coverage radius versus altitude of UB_v of scotopic designed RGB LED for varying illuminance threshold at 1 W transmitted optical power.

Fig. 12 displays the coverage radius versus altitude for night scenario considering scotopic case designed RGB LED (as discussed in section III-A2) at 1 W transmitted optical power for different illuminance threshold. The trend of first increasing and then decreasing r with respect to L remains the same. However, r has increased from the photopic case, which indicates that with RGB LED based energy-aware technique, the coverage radius can be increased without increasing the transmitted optical power. The reason behind increased r is the higher lumens/watt perceived by the human eye at night. The practical design of RGB LED makes it feasible to support the maximum possible lumens/watt while maintaining white tone light which ultimately increases the luminous efficacy and thus illuminance.

Fig. 13 presents the effect of transmitted optical power on UB_v altitude and its r at 13 dB SNR threshold. It is evident from (1) that SNR is directly proportional to transmitted optical power. Therefore, on increasing P_t, the coverage radius increases. However, this work aims to increase r with sustainable and energy-aware techniques. Therefore, the utilization of holographic LSD and RGB LED based solutions have been proposed to support green communication through UB_v. Moreover, from Figs. 10 and 13, we can interpret that r increases more for lower SNR thresholds. The values of maximum coverage radius have been obtained analytically using (8) for different P_t.

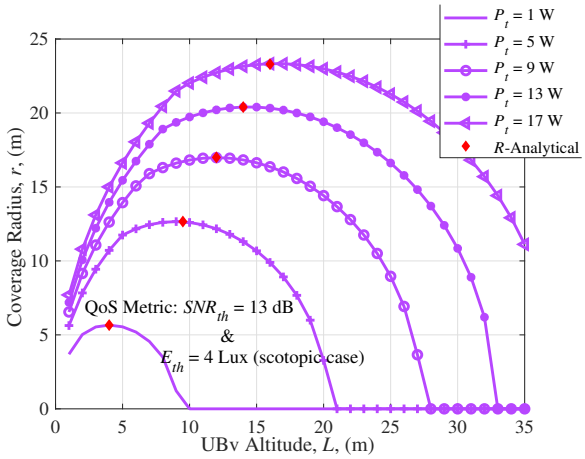

Fig. 14. Coverage radius versus altitude of UB_v considering SNR and illuminance threshold at different transmitted optical power.

In Fig. 14, UB_v altitude and its coverage radius has been plotted considering both QoS metrics i.e. SNR and illuminance at different P_t. The results have been obtained for scotopic case. Since, during day scenario only SNR QoS metrics is considered (as shown in Fig. 13 and already discussed in section II-B). The peak of UB_v coverage radius and altitude range decreases further from results in Fig. 13 owing to illuminance threshold. The minimum of $[r_{SNR}, r_E]$ obtained from (8) and (9), respectively, provides R analytically. However, for scotopic case utilizing RGB LED based solution, the V_λ in (9) is replaced with V_λ^{rgb} as shown in (12).

Fig. 15 shows the plot of received power distribution in 2-D versus coverage radius in the x-axis of the user's plane with

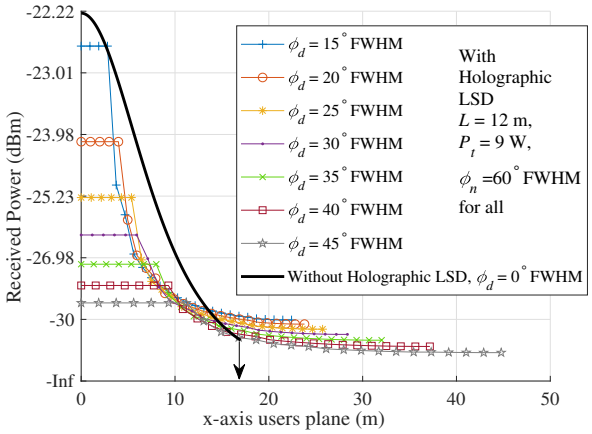

Fig. 15. Relation of Coverage radius with varying holographic LSD angle of FOV at 9W transmitted optical power.

varying ϕ_d of the holographic LSD at 9 W transmitted optical power. The black-lined plot displays the received power distribution without holographic LSD. The tail of all the plots ends at a certain x-axis of the user's plane, which connotes that there is no further coverage after that. This has been visually shown for the black-lined plot with a downward arrow. It is observed that as ϕ_d increases, the received power distribution becomes more uniform till a higher coverage radius. Nevertheless, this comes with a penalty of decreased received power at the user's plane. As ϕ_d increases, the effective output angle in (10) also increases which finally increases the coverage. Moreover, with larger ϕ_e the light diffuses more, so the average of the sum of individual footprints per pixel provides decreased received power.

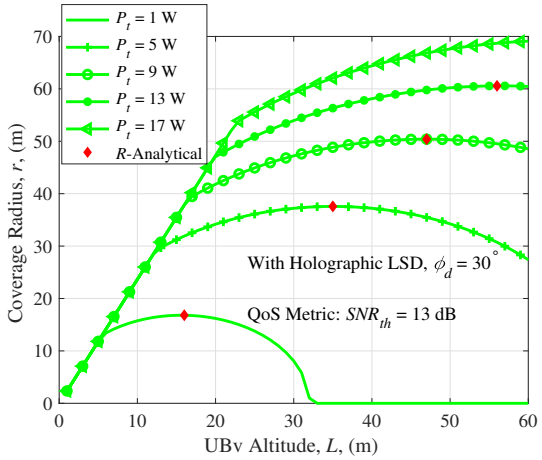

Fig. 16. Coverage radius versus altitude of UB_v considering SNR threshold and holographic LSD at different transmitted optical power.

Fig. 16 presents UB_v coverage radius with respect to its altitude considering SNR threshold and holographic LSD at different transmitted optical power. It is observed that as compared to Fig. 13, the coverage radius and altitude range has significantly increased with the adoption of holographic LSD at LED front end. The minimum of [$r'_{SNR}(L_o^{SNR})$,$r_{LSD}(L_o^{SNR})$], obtained from (16) and (11), respectively, provides R analytically. The second order differentiation of (16) is derived to obtain the maximum value of altitude L_o^{SNR}. The altitude L_o^{SNR} is used in (16) and (11) to obtain respective coverage radius and finally the minimum among them becomes the R. The analytical results match well with the peak value of the simulation results.

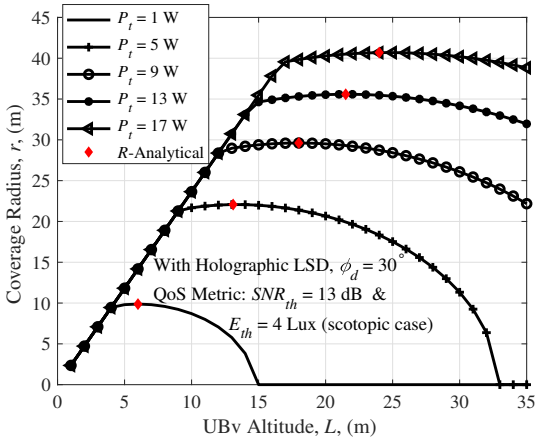

Fig. 17. Coverage radius versus altitude of UB_v considering SNR and illuminance threshold with holographic LSD at different transmitted optical power.

Lastly, in Fig. 17, UB_v coverage radius and its altitude has been plotted considering SNR and illuminance threshold with holographic LSD for different P_t. It is observed that as compared to Fig. 14, the coverage radius and altitude range has significantly increased due to the holographic LSD. However, as compared to the results in Fig. 16, the coverage radius and altitude range reduce, which can be attributed to the illuminance threshold. The minimum of the four different optimized r as seen in (17) provides the maximum coverage radius with enhanced coverage area satisfying both E_{th} and SNR_{th}. Consequently, R is obtained analytically. The analytical results show good agreement with the peak value of the simulation results validating the derived analytical expressions.

We have analytically obtained and shown L_o and R at varying P_t in Fig. 17. However, the L_o and R can be obtained by varying different parameters as well such as SNR_{th} and E_{th}. Table III presents the value of L_o and its respective R for the proposed work considering varying SNR and illuminance threshold at night scenario with $P_t = 9$ W. It is observed that as E_{th} increases for varying values of SNR_{th}, L_o and R decreases and depends more on E_{th} than SNR_{th}, which is due to the increased limit imposed by E_{th}. Similarly, as SNR_{th} increases for varying values of E_{th}, L_o and R decreases which is obvious due to the increased SNR threshold value. However, from $E_{th} = 8$ Lux onwards, the L_o and R does not change even for varying SNR_{th}, which again shows the higher limit imposed by E_{th} than SNR_{th} on L_o and R. This has already been observed and discussed above while comparing Fig. 16 and Fig. 17. However, with the rigorous analytical results of Table III, it has become more clear that L_o and R are more limited by E_{th} than SNR_{th}. Further, at $P_t = 9$ W, E_{th} = 4 Lux and SNR_{th} = 13 dB, the L_o and R values are 17.9 m and 29.7 m, respectively which perfectly matches with the black circle marker plot (i.e. at $P_t = 9$ W) of Fig. 17.

TABLE III
RESULTS OF ANALYTICAL SOLUTION FOR R AT $P_t = 9$ W CONSIDERING VARYING SNR AND ILLUMINANCE THRESHOLD WITH HOLOGRAPHIC LSD FOR NIGHT SCENARIO.

Parameter:	E_{th} = 1 Lux		E_{th} = 4 Lux		E_{th} = 16 Lux	
SNR_{th} (dB)	L_o (m)	R (m)	L_o (m)	R (m)	L_o (m)	R (m)
10	43.5	58.5	17.9	29.7	9	14.8
13	46.9	50.4	17.9	29.7	9	14.8
16	39.5	42.4	17.9	29.7	9	14.8
20	31.4	33.7	17.9	29.7	9	14.8
25	23.5	25.3	23.5	25.3	9	14.8
Parameter:	SNR_{th} = 10 dB		SNR_{th} = 13 dB		SNR_{th} = 25 dB	
E_{th} (Lux)	L_o (m)	R (m)	L_o (m)	R (m)	L_o (m)	R (m)
1	43.5	58.5	40.9	50.4	23.5	25.3
4	17.9	29.7	17.9	29.7	23.5	25.3
8	12.7	20.9	12.7	20.9	12.7	20.9
12	10.4	17.1	10.4	17.1	10.4	17.1
16	9	14.8	9	14.8	9	14.8

TABLE IV
SIMULATION PARAMETERS.

Parameter	Value	Parameter	Value
v_u	1.5 m/s	N	20
v_{uav}	25 m/s	$fair_{thres}$	0.7
σ	4 m	t_{min}	4 s
L_o	17.9 m	t_{max}	50 s
T	600 s	Simulated Area	200 × 200 sq. m

From the aforementioned analysis and discussion, a network engineer can finalize the optimum altitude for maximum coverage radius based on the network's application and requirement while supporting green communication and network. For instance, if it is decided to achieve the maximum coverage radius of 30 m in the night scenario with an optical power constraint of 9 W, then without LSD and RGB LED, the engineer would have no choice but to increase the P_t beyond 17 W. However, with the proposed enhancement techniques, i.e., LSD and RGB LED, the engineer can achieve $R = 30$ m with lower P_t (see Fig. 17), which support the energy-aware aspect of green communication and network. To achieve this aim, at first optimal altitude is obtained from the relation between UB_v altitude and its coverage radius considering both QoS metrics at $P_t = 9$ W as shown in Fig. 14. After that, $\phi_d = 30°$ FWHM is chosen based on the plot of received power distribution and the x-axis of the user's plane as presented in Fig. 15. Further, the relation between UB_v coverage radius and its altitude is obtained considering both SNR and illuminance threshold with holographic LSD for night scenario and only SNR threshold with holographic LSD for day scenario at designated P_t. For night scenario, R approaches close to 30 m in Fig. 17 and for day scenario, the maximum coverage radius approaches close to 50 m as seen in Fig. 16. Further, with the proposed analytical solution, a network engineer has freedom to fix and vary parameters of his interest to directly deduce L_o and R for a given QoS metric .

Finally, the maximum coverage radius obtained is 29.7 m for the night scenario. Going ahead with $R = 29.7$ m, we present the results of the iterative solution to problems P1 and P2. In our study, all the users are initially considered inside

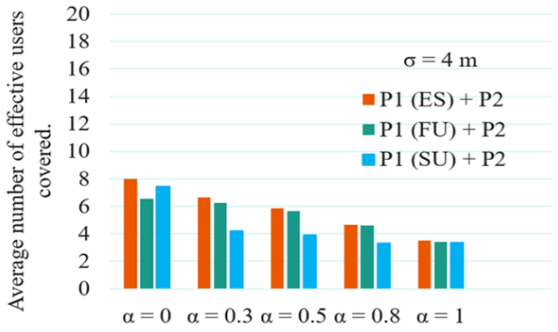

Fig. 18. Average number of users covered at $T = 600$ seconds at $N = 20$.

the UB_v's coverage area. The initial placement of UB_v is at the optimum altitude just above the center of the users' plane as shown in Fig. 5. Further, we assume that the first UB_v placement update occurs after t_{min} seconds. The first update interval $t_{up}(1)$ and optimal UB_v placement is obtained after solving P1 and P2 iteratively. After this, the UB_v placement is updated at $(t_{min} + t_{up}(1))$ seconds. This process goes on till the total UB_v operation time, i.e., T seconds. The results are averaged over 50 UB_v operation periods. The simulation parameters are mentioned in Table IV.

Fig. 18 presents the average effective number of users covered per update interval in the UB_v network for $T = 600$ s. As α increases for all three methods, the number of users covered decreases. It is because less frequent UB_v placement updates result in lower coverage probability. Figs. 19 and 20 show the average number of update instants and average update interval, at $\sigma = 4$ m for all the three methods, respectively. With an increase in α, the number of update instants reduce, and update intervals increase. It is because an increase in α ensues more weightage to minimize the total UB_v flight time in (24). It causes less frequent UB_v placement updates and thus increases the update interval, thereby reducing energy consumption and making the deployment more energy efficient.

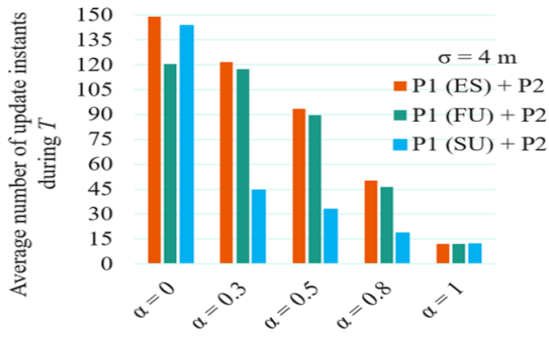

Fig. 19. Average number of update instants during $T = 600$ seconds.

In Figs. 18-20, the results of FU and SU method equals ES method at $\alpha = 1$. The reason is the proposed optimization problem (24), where at $\alpha = 1$, the minimization problem does not have a coverage probability factor. Therefore, P2 when left with the minimization of total UB_v flight time only, the number of update instants reduces significantly (see Fig. 19) and update interval increases drastically (refer Fig. 20).

This article has been accepted for publication in a future issue of this journal, but has not been fully edited. Content may change prior to final publication. Citation information: DOI 10.1109/TGCN.2022.3171920, IEEE Transactions on Green Communications and Networking

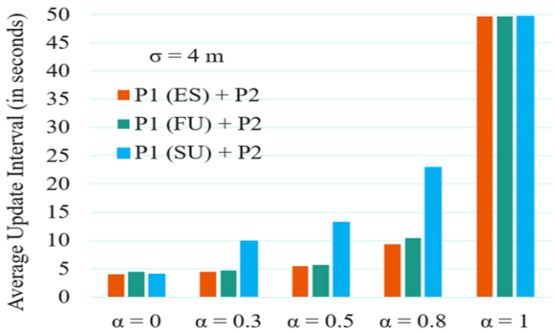

Fig. 20. Average update interval at $T = 600$ seconds.

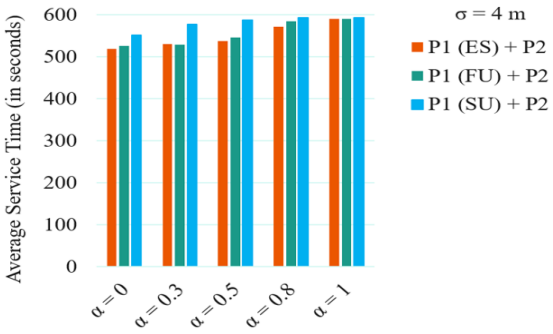

Fig. 21. Average service time at $T = 600$ seconds.

With this, the iterative solution of P1 and P2 approaches similar values despite different solving methods. Therefore, in Fig. 18, the average number of effective users covered in the FU and SU method approaches the ES method. Besides, it is observed in Figs. 18-20 that for $\alpha = 0.3, 0.5, 0.8$, the results of FU method approaches close to ES method. Since the FU method is the truncated version of ES by farthest user, as the weightage of α incorporates minimization of fly time along with coverage probability, it approaches close to the ES method. However, in Fig. 18 for $\alpha = 0.3, 0.5, 0.8$, SU method provides less $\bar{U_e}$ as compared to ES method and this is due to Algorithm 2 where UB_v is shifted as per uncovered users which limits the possibility of covering users under constraint C2. Similarly, in Fig. 19, the number of update instants in the SU method is significantly lower than the other two methods. Hence, UB_v changes its position less frequently with the SU method, thereby reducing energy consumption and making the deployment more energy efficient. The lower number of update instant and higher update intervals of SU method in Fig. 20 leads to lower $\bar{U_e}$. The probability of the user moving outside the UB_v coverage area increases at a higher update interval. Consequently, for each user, coverage probability decreases with an increase in t_{up}. Moreover, in Figs. 18-20 at $\alpha = 0$, there is no minimization of fly time; hence the ES method updates frequently to cover the maximum possible number of users. However, the FU method can update hover points till the area defined by the farthest user at k^{th} update instant, which reduces the update frequency. Further, for $\alpha = 0$ SU method approaches ES method, as UB_v can shift anywhere within C1 and C2 constraints with the sole aim to maximize coverage probability.

Fig. 21 presents the average service time (i.e., average hovering time) for varying α. It can be observed that with an increase in α, average service time increases. Since in the FU method, $\bar{U_e}$ is slightly lower than the ES method due to a slightly reduced number of update instants. Therefore, in Fig. 21, we can observe slight higher $\mathcal{S}$ than ES method for all α value except zero. The reason behind almost exact value at $\alpha = 0$ for all the three methods has already been discussed above. Further, in the SU method, $\mathcal{S}$ is higher for most of the α due to the fewer number of update instants (as shown in Fig. 19) as compared to the ES method.

It should be noted that for the SU method, constraint C1 is relaxed with a delta value (δ) in $fair_{thres}$ so as to avoid the non-feasible solution set and proceed further with the iterative solution of P1 and P2 based on uncovered users only. The fairness threshold now becomes $fair_{thres} - \delta$. Table V shows the error margins, i.e., the average percentage of times (error %) $fair_k$ does not follow strict C1 as per (22) and the average delta value considered at $fair_k$ for T seconds. It is observed that the error margins are very less. Further, the results of Figs. 18 and 21 for all the three methods has been compiled in Table VI for clear comparison. Fig. 22 depicts the complexity of ES, FU and SU methods which has been explained in detail in section III-D.

TABLE V
SU METHOD ERROR MARGIN.

α	error %	δ
0	1.06 %	0.0075
0.3	2.41 %	0.0082
0.5	0.69 %	0.0077
0.8	0.46 %	0.0052
1	0.1 %	0.0140

The aim of this work is that eventually, a network engineer can take insight from the above-discussed results and tune α based on the requirement to cover more users or provide a larger service time with user mobility and energy awareness. Further, SU method can be chosen for optimal UB_v placement when time complexity thus energy required at UB_v is a big issue and the network engineer is ready to compromise in $\bar{U_e}$ with slight error margin as inferred from Tables V-VI and Fig. 22. The decimal values of $\bar{U_e}$ in Table VI implies that at $t_{up}(k)$ update interval few users are covered for time duration less than $t_{up}(k)$. Moreover, SU can be preferred to provide higher service time with energy efficiency over ES and FU methods. However, the FU method can be considered when the network engineer can not compromise on the number of covered users as it provides coverage close to the ES method with less energy and time complexity.

V. CONCLUSION

This work optimizes the 3-D placement of UB_v and update interval while maintaining illuminance and SNR threshold. Initially, the optimal altitude is determined based on the maximum coverage radius of UB_v considering the QoS metrics depending on day and night scenario. The coverage radius has been enhanced with holographic LSD with the motive of adopting an energy-aware and greener aspect of communication. Further, a novel RGB LED-based solution has

TABLE VI
AVERAGE EFFECTIVE NUMBER OF USERS COVERED AND AVERAGE TOTAL SERVICE TIME FOR ES, FU AND SU METHOD.

α	U_e	$\mathcal{S}$
ES Method:		
0	8.01	519.10 s
0.5	5.83	537.65 s
1	3.50	590.70 s
FU Method:		
0	6.54	526.07 s
0.5	5.64	546.30 s
1	3.41	590.16 s
SU Method:		
0	7.47	552.65 s
0.5	4.00	587.64 s
1	3.36	59.68 s

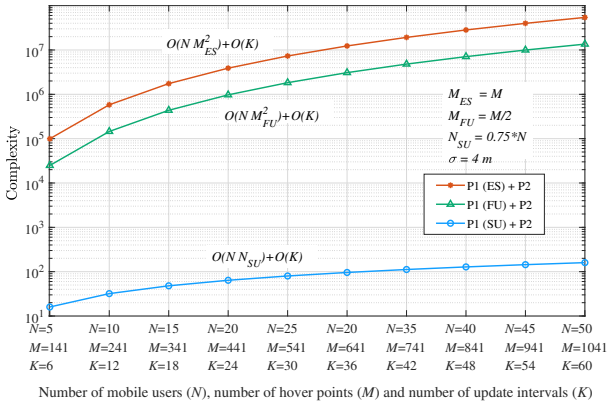

Fig. 22. Computational complexity of solving P2 and P1 with different algorithms.

been proposed for the night scenario considering the human eye's light sensitivity to increase the illuminance and thus coverage radius. The maximum coverage radius thus obtained for the scotopic case without any enhancements and with the proposed energy-aware enhancements is 16.98 m and 29.7 m, respectively. The proposed enhancements increase the coverage area of UB_v by 207%. Additionally, the analytical solution has been provided to obtain the maximum coverage radius and its optimal altitude with the proposed enhancements techniques. Subsequently, the joint optimization of 2-D UB_v placement and update interval to maximize the number of covered users and minimize UB_v flight time at an update instant while accounting for the user fairness has been proposed. The proposed FU and SU methods to solve the objective function achieve performance close to the exhaustive-search method with reduced complexity. The effective number of users covered by the SU method at $\alpha = 0.5$ is 4, the least among all the three methods. However, selecting the SU method is an energy-aware decision to achieve a greener network since it provides the maximum service time and drastically reduced time complexity compared to the FU and ES methods. Further, the proposed analysis can be extended to multi-UB_v communication network and the fair maximum coverage problem can be solved using reinforcement learning; however, that will be the subject of future work.

REFERENCES

[1] A. Fotouhi, H. Qiang, M. Ding, M. Hassan, L. G. Giordano, A. Garcia-Rodriguez, and J. Yuan, "Survey on uav cellular communications: Practical aspects, standardization advancements, regulation, and security challenges," *IEEE Commun. Surv. Tut.*, vol. 21, no. 4, pp. 3417–3442, Fourthquarter 2019.

[2] Y. Zeng, Q. Wu, and R. Zhang, "Accessing from the sky: A tutorial on uav communications for 5g and beyond," *Proceedings of the IEEE*, vol. 107, no. 12, pp. 2327–2375, Dec. 2019.

[3] N. Chi, H. Haas, M. Kavehrad, T. D. C. Little and X. Huang, "Visible light communications: demand factors, benefits and opportunities," *IEEE Wirel. Commun.*, vol. 22, no. 2, pp. 5–7, Apr. 2015.

[4] H. Haas, L. Yin, Y. Wang and C. Chen, "What is LiFi?," *J. Lightw. Technol.*, vol. 34, no. 6, pp. 1533-1544, Mar. 2016.

[5] Y. Tanaka, S. Haruyama, and M. Nakagawa, "Wireless optical transmissions with white colored LED for wireless home links," in *Proc. IEEE 11th Symp. Pers. Indoor Mobile Radio Commun. (PIMRC)*, London, UK, Sept. 2000, pp. 1325–1329.

[6] H. Deng, J. Li, A. Sayegh, S. Birolini, and S. Andreani, "Twinkle: A flying lighting companion for urban safety," in *Proc. of the ACM 12th Int. Conf. Tangible, Embedded, Embodied Interaction*, Stockholm, Sweden, Mar. 2018, pp. 567–573.

[7] Draganfly, [Online]. Available: https://draganfly.com/

[8] Y. Yang, M. Chen, C. Guo, C. Feng, and W. Saad, "Power efficient visible light communication with unmanned aerial vehicles," *IEEE Commun. Lett.*, vol. 23, no. 7, pp. 1272–1275, 2019.

[9] Z. Zhu, Y. Yang, C. Guo, M. Chen, S. Cui and H. V. Poor, "Power efficient deployment of VLC-enabled UAVs," in *IEEE 31st Annual Int. Symp. Pers. Indoor Mobile Radio Commun. (PIMRC)*, London, UK, Sept. 2020, pp. 1-6.

[10] A. Singh, D. N. Anwar, A. Srivastava, V. A. Bohara, and G. S. VRK Rao "Power and SER analysis of VLC- and RF-based links in indoor environment", in *SPIE 10945, Broadband Access Commun. Technol. XIII*, Feb. 2019, p. 109450R.

[11] M. Obeed, A. M. Salhab, M. -S. Alouini and S. A. Zummo, "On optimizing VLC networks for downlink multi-user transmission: a survey," *IEEE Commun. Sur. Tut.*, vol. 21, no. 3, pp. 2947-2976, thirdquarter 2019.

[12] F. Lagum, I. Bor-Yaliniz, and H. Yanikomeroglu, "Strategic densification with uav-bss in cellular networks," *IEEE Wirel. Commun. Lett.*, vol. 7, no. 3, pp. 384–387, Jun. 2018.

[13] C. Zhan, Y. Zeng, and R. Zhang, "Trajectory design for distributed estimation in uav-enabled wireless sensor network," *IEEE Trans. Veh. Technol.*, vol. 67, no. 10, pp. 10 155–10 159, Oct. 2018.

[14] M. Peer, V. A. Bohara, A. Srivastava, and G. Ghatak, "User mobility aware time stamp for uav-bs placement," in *IEEE Wirel. Commun. Netw. Conf. Workshops (WCNCW)*, Mar. 2021, pp. 1–6.

[15] Lecture notes, "COMPSCI 530: Design and analysis of algorithms," chapter 16 slides, Fall 2013, Computer Science and Engineering Department, Duke University, North Carolina, [Online]. Available: https://courses.cs.duke.edu//fall13/compsci530/notes/lec16.pdf.

[16] L. Liu, S. Zhang, and R. Zhang, "Comp in the sky: UAV placement and movement optimization for multi-user communications," *IEEE Trans. Commun.*, vol. 67, no. 8, pp. 5645–5658, Aug. 2019.

[17] R. Ghanavi, E. Kalantari, M. Sabbaghian, H. Yanikomeroglu, and A. Yongacoglu, "Efficient 3D aerial base station placement considering users mobility by reinforcement learning," in *IEEE Wirel. Commun. Netw. Conf. (WCNC)*, Barcelona, Spain, Apr. 2018, pp. 1–6.

[18] X. Liu, Y. Liu, Y. Chen, and L. Hanzo, "Trajectory design and power control for multi-uav assisted wireless networks: A machine learning approach," *IEEE Transactions on Vehicular Technology*, vol. 68, no. 8, pp. 7957–7969, 2019.

[19] H. V. Abeywickrama, Y. He, E. Dutkiewicz, B. A. Jayawickrama, and M. Mueck, "A reinforcement learning approach for fair user coverage using uav mounted base stations under energy constraints," *IEEE Open J. Veh. Technol.*, vol. 1, pp. 67–81, Feb. 2020.

[20] J. Wang, C. Jiang, Z. Han, Y. Ren, R. G. Maunder and L. Hanzo, "Taking drones to the next level: cooperative distributed unmanned-aerial-vehicular networks for small and mini drones," *IEEE Veh. Technol. Mag.*, vol. 12, no. 3, pp. 73-82, Sept. 2017.

[21] Y. Wang, M. Chen, Z. Yang, T. Luo, and W. Saad, "Deep learning for optimal deployment of UAVs with visible light communications," *IEEE Trans. Wirel. Commun.*, vol. 19, no. 11, pp. 7049– 7063, Nov. 2020.

[22] Q.-V. Pham, T. Huynh-The, M. Alazab, J. Zhao, and W.-J. Hwang, "Sum-rate maximization for uav-assisted visible light communications using noma: Swarm intelligence meets machine learning," *IEEE Internet Things J.*, vol. 7, no. 10, pp. 10 375–10 387, Oct. 2020.

[23] Luminit, "Technical data sheet on light shaping diffusers," USA, 2012. [Online]. Available: https://www.luminitco.com/sites/default/files/LSD_Tech_Datasht_5_21_12_lo_0.pdf

[24] D. Wu, Z. Ghassemlooy, H. Le-Minh, S. Rajbhandari, and L. Chao "Channel characteristics analysis of diffuse indoor cellular optical wireless communication systems", in *proc. SPIE 8309, Opt. Transmission Syst., Subsystems, Technol. IX*, Shanghai, China, Dec. 2011, p. 83090P.

[25] D. Wu, Z. Ghassemlooy, H. LeMinh, S. Rajbhandari and Y. S. Kavian, "Power distribution and Q-factor analysis of diffuse cellular indoor visible light communication systems," in *proc. 16th European Conf. Netw. Opt. Commun.*, Newcastle upon Tyne, UK, Jul. 2011, pp. 28-31.

[26] M. A. Boon, A. P. Drijfhout, and Solomon Tesfamichael, "Comparison of a fixed-wing and multi-rotor uav for environmental mapping applications: A case study," *Int. Arch. Photogramm. Remote Sens. Spat. Inf. Sci. (ISPRS)*, vol. 42, p. 47, Aug. 2017.

[27] M. Mozaffari, W. Saad, M. Bennis, Y. H. Nam and M. Debbah, "A tutorial on UAVs for wireless networks: applications, challenges, and open problems," *IEEE Commun. Surv. Tut.*, vol. 21, no. 3, pp. 2334-2360, thirdquarter 2019.

[28] Y. Qiu, H.-H. Chen, and W.-X. Meng, "Channel modeling for visible light communications: a survey," *Wireless Commun. Mob. Comput.*, vol. 16, no. 14, pp. 2016–2034, Oct. 2016.

[29] J. M. Kahn and R. J. Barry. "Wireless infrared communications," *Proc. of the IEEE*, vol. 85, no. 2, pp. 265-298, Feb. 1997.

[30] M. A. Arfaoui, M. D. Soltani et al., "Measurements-Based Channel Models for Indoor LiFi Systems," *IEEE Trans. Wireless Commun.*, vol. 20, no. 2, pp. 827-842, Feb. 2021.

[31] D. N. Anwar, R. Ahmad and A. Srivastava, "Energy-Efficient Coexistence of LiFi Users and Light Enabled IoT Devices," *IEEE Trans. Green Commun. Netwo.*, Sep. 2021, doi: 10.1109/TGCN.2021.3116267.

[32] T. Komine and M. Nakagawa, "Fundamental analysis for visible-light communication system using led lights," *IEEE trans. Consum. Electron.*, vol. 50, no. 1, pp. 100–107, Feb. 2004.

[33] I. Din and H. Kim, "Energy-efficient brightness control and data transmission for visible light communication," *IEEE photon. technol. lett.*, vol. 26, no. 8, pp. 781–784, Apr. 2014.

[34] HyperPhysics: Light and Vision [Online]. Available: http://hyperphysics.phy-astr.gsu.edu/hbase/vision/efficacy.html#c1

[35] A. Sarkar, S. K. Singh, N. Jain, and V. Dwidedi, "India-energy-efficient street lighting: implementation and financing solutions," The World Bank, Tech. Rep., 2015.

[36] Yiguang Wang, Xingxing Huang, Jianyang Shi, Yuan-quan Wang, and Nan Chi, "Long-range high-speed visible light communication system over 100-m outdoor transmission utilizing receiver diversity technology," *SPIE: Optical Engineering*, vol. 55, no. 5, p. 056104, May 2016.

[37] P. Cherntanomwong and P. Namonta, "The repeater system for visible light communication," in *proc. 7th Int. Conf. Inf. Technol. Elect. Eng. (ICITEE)*, Chiang Mai, Thailand, Oct. 2015, pp. 489-493.

[38] P. Namonta and P. Cherntanomwong, "The improvement of repeater system for visible light communication," in *proc. 13th Int. Conf. Elect. Eng./Electron., Comp., Telecommun. Inf. Technol. (ECTI-CON)*, Chiang Mai, Thailand, Jun.-Jul. 2016, pp. 1-6.

[39] D. N. Anwar and A. Srivastava, "Constellation design for single photodetector based CSK with probabilistic shaping and white color balance," *IEEE Access*, vol. 8, pp. 159609-159621, Aug. 2020.

[40] *IEEE standard for local and metropolitan area networks-Part 15.7: Short-range optical wireless communications*, IEEE Std 802.15.7-2018 (Revision of IEEE Std 802.15.7-2011), pp.1-407, Apr. 2019.

[41] R. Jain, D.-M. Chiu, and W. R. Hawe, *A quantitative measure of fairness and discrimination for resource allocation in shared computer system*, Hudson, MA, USA: Eastern Research Laboratory, Digital Equipment Corporation, 1984, vol. 38.

[42] Y. Zeng, J. Xu, and R. Zhang, "Energy minimization for wireless communication with rotary-wing uav," *IEEE Trans. Wirel. Commun.*, vol. 18, no. 4, pp. 2329–2345, Apr. 2019.

[43] A. Asudeh, T. Berger-Wolf, B. DasGupta, and A. Sidiropoulos, "Maximizing coverage while ensuring fairness: a tale of conflicting objective," *arXiv preprint arXiv:2007.08069*, Jul. 2020.

[44] G. Laporte, "The traveling salesman problem: An overview of exact and approximate algorithms," *Eur. J. Oper. Res.*, vol. 59, pp. 231–247, Jun. 1992.

[45] L. Siklóssy, E. Tulp, "The space reduction method: a method to reduce the size of search spaces," *Inf. Processing Lett.*, vol. 38, pp. 187-192, May 1991.

[46] S. Arora, "Polynomial time approximation schemes for euclidean traveling salesman and other geometric problems," *J. ACM*, vol. 45, pp. 753-782, Sep. 1998.

[47] V. Vazirani, *Approximation Algorithms*, 1st ed., Berlin: Springer, 2001.

[48] A. J. Martin, "Towards an energy complexity of computation," *Inf. Process. Lett.* 77.2-4, pp. 181-187, Feb. 2001.

[49] R. Jain, D. Molnar, and Z Ramzan, "Towards a model of energy complexity for algorithms," in *proc. IEEE Wirel. Commun. Netw. Conf.*, New Orleans, LA, USA, Mar. 2005, vol. 3, pp. 1884-1890.

[50] T. H. Cormen, C. E. Leiserson, R. L. Rivest and C. Stein, *Introduction to Algorithms*, 3rd ed., Cambridge, England: MIT Press, Massachusetts, London, 2009.